Scanning Electrochemical Microscopy (SECM) with Amalgam Microelectrodes

A Thesis
Presented to
The Academic Faculty
by

Douglas Alexander Rudolph

In Partial Fulfillment
of the Requirements for the Degree
Master of Science in Chemistry

School of Chemistry and Biochemistry
Georgia Institute of Technology
August 2005

Scanning Electrochemical Microscopy (SECM) with Amalgam Microelectrodes

Approved by:

Dr. Boris Mizaikoff, Chair
School of Chemistry and Biochemistry
Georgia Institute of Technology

Dr. Jiri Janata
School of Chemistry and Biochemistry
Georgia Institute of Technology

Dr. Thomas DiChristina
School of Biology
Georgia Institute of Technology

Date Approved: May 19, 2005

ACKNOWLEDGEMENTS

I would like to thank Dr. Boris Mizaikoff and Dr. Christine Kranz for all of their support and knowledge while conducting this research. I would also like to thank the members of the ASL group, Taillefert group, and DiChristina group.

Stephanie Nuehuber

Markus Janotta

Nick Mendegazzo

David Bates

Gary Dobbs

I acknowledge support for this research from the National Science Foundation (Biocomplexity/IDEA project #0216368 and IGERT "Signals in the sea" project #0114400).

Finally, I would like to thank my family and friends for all of their love and support.

TABLE OF CONTENTS

LIST OF TABLES

LIST OF FIGURES

SUMMARY

This thesis focuses on in-situ studies at the solid-liquid interface by combining scanning electrochemical microscopy (SECM) with gold and platinum mercury amalgam microelectrodes. It is shown that stripping voltammetry experiments at imaging amalgam microelectrodes provide laterally resolved insight on the electrochemistry of biogeochemically relevant processes. SECM provides information on electroactive surface processes with high spatial resolution, and offers the opportunity to study heterogeneous electron-transfer reactions. Thereby, chemical species of interest, such as metal ions, can be electrochemically detected at mercury amalgam electrodes.

Platinum and gold mercury amalgam microelectrodes were developed for the detection of biogeochemically relevant analytes such as manganese and iron during SECM imaging experiments at the mineral/water interface establishing the fundamental basis of SECM imaging with amalgam microelectrodes.

SECM experiments were performed for the quantitative determination of Mn^{2+} during the dissolution of microstructured manganese carbonate ($MnCO_3$; rhodochrosite) precipitates at mildly acidic conditions. SECM images along with spatially resolved quantitative data on the Mn^{2+} concentration were obtained.

This measurement concept was then extended to the investigation of the corrosion behavior of diamond-like carbon (DLC) protected zinc selenide (ZnSe) waveguides applied in mid-infrared attenuated total reflectance spectroscopy at strongly oxidizing conditions. The corrosion behavior of DLC coated and uncoated ZnSe crystals was studied obtaining laterally resolved information on the oxidative degradation of ZnSe at defects of the DLC layer utilizing SECM in combination with square wave anodic

stripping voltammetry (SWASV) at gold amalgam microelectrodes. Thereby, insight on the corrosion behavior of ZnSe and concentration profiles of Zn^{2+} at oxidizing conditions was obtained. These results corroborate the utility of SECM imaging with amalgam microelectrodes for addressing relevant analytical questions.

Finally, the developed amalgam microelectrodes were applied for SECM studies of iron-reducing proteins separated from *Shewanella* microbes in native polyacrylamide gels. After calibration of Pt/Hg microelectrodes in bulk solution for the targeted analytes (iron and sulfur species), SECM approach curves recorded above the native gel enabled positioning of the amalgam electrode in close proximity above protein bands with suspected iron-reducing activity. This technique enabled the (semi)quantitative determination of the anaerobic respiratory activity associated with microbial proteins/protein complexes responsible for the reductive dissolution of manganese and iron oxides above microbial protein bands separated in a native gel matrix.

1. INTRODUCTION AND MOTIVATION

1.1 Contribution to Biocomplexity in the Environment

The ability to simultaneously obtain chemical and topographical information will significantly enhance our knowledge of complex biological systems at the molecular level. Scanning probe microscopy techniques provide a family of analytical tools for obtaining topographical and chemical information with high spatial resolution. Each technique – scanning tunneling microscopy (STM), atomic force microscopy (AFM), and scanning electrochemical microscopy (SECM) – is designed to provide a specific type of data. While AFM and STM provide superior spatial resolution, they are usually deficient in chemical specificity, which is uniquely provided by SECM rendering it an ideal tool for bioanalysis. Scanning electrochemical microscopy (SECM) is a scanning probe technique which can provide electrochemical information at the microscale.

The scanning electrochemical microscope (SECM) was introduced in 1986 by Bard et al. and Engstrom et al. as an instrument capable of examining chemistry at high resolution near interfaces (Bard et al., 1986; Engstrom et al., 1986). SECM can be utilized to obtain chemical reactivity images of surfaces, but also for quantitative measurements of reaction rates. SECM has been used for a wide range of applications, including studies of corrosion, biological systems (e.g. enzymes), membranes, solid dissolution, and liquid/liquid interfaces (Bard, Fan, & Mirkin, 1994).

In general, SECM combines electroanalytical measurements techniques with the principle of scanning a microelectrode in close proximity across a sample surface. During SECM experiments, information on local electrochemical activity is provided by the disturbance of Faraday currents at a scanned biased microelectrode. A disk

microelectrode with diameters ranging from 1 to 25 μm is typically used. Microelectrodes have advantages over macroelectrodes due to their reduced size, reduced double layer charging effects, well defined steady state currents, and a reduced ohmic drop enabling their application as scanning probes. The obtained Faraday current at a microelectrode is a function of the tip-sample distance (Kwak & Bard, 1989).

As is other types of scanning probe microscopies, SECM is based on the movement of a very small electrode (tip) near the surface of a conductive or insulating substrate. In amperometric SECM experiments, the tip is usually a conventional ultramicroelectrode (UME) fabricated as a conductive disk of metal in an insulating sheath of glass. The tip current is perturbed by the presence of the substrate. When the tip is far (i.e. > several tip diameters) from the substrate, the steady-state current, $i_{T,\infty}$, is given by equation 1.

$$i_{T,\infty} = 4nFDCa \qquad (1)$$

F is the Faraday constant, n the number of electrons transferred in the tip reaction, D the diffusion coefficient of the redox mediator used, C is the concentration of the mediator, and a is the tip radius. During SECM imaging, the microelectrode tip is positioned in close proximity (i.e. within 1-2 electrode radii) to the sample surface by recording current-distance curves ("approach curves"). When the tip is moved toward an insulating surface, the tip current, i_T, decreases because the insulating sheath of the tip blocks diffusion of the redox mediator to the tip from the bulk solution. The closer the tip gets to the substrate, the smaller i_T becomes (negative feedback, Figure 1(a)). Above a conductive substrate, the redox mediator can be re-oxidized. This produces an additional flux of re-oxidized mediator to the tip and, hence, an increase in tip current (positive

feedback, Figure 1(b)). These principles are the basis for the feedback mode of SECM (Kwak & Bard, 1989).

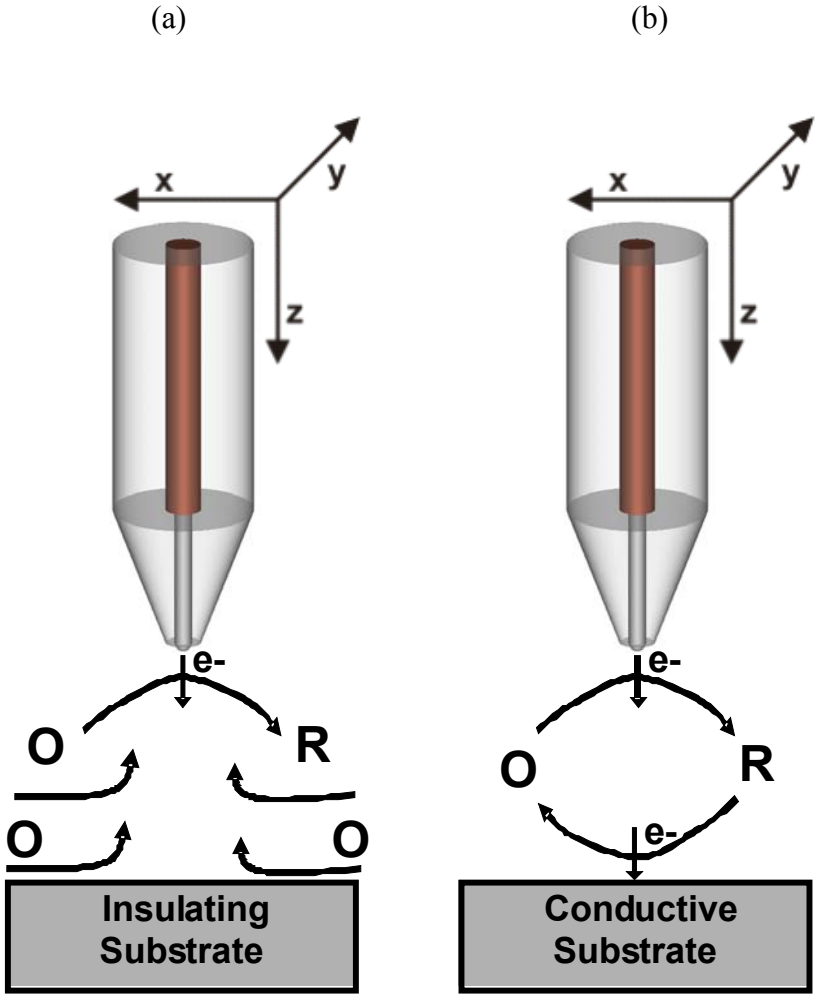

Figure 1: Operating principles of SECM: (a) UME near an insulating substrate: hindered diffusion of O leads to $i_t < i_{T,\infty}$ (negative feedback). (b) UME near a conductive substrate: positive feedback of O leads to $i_T > i_{I,\infty}$.

In the feedback mode of SECM, the overall redox process is confined to the thin layer between the tip and substrate. In the generation / collection mode (considering the substrate is the generator and the tip is the collector), the tip moves within a thin diffusion layer generated by the substrate (Kwak & Anson, 1992). In this mode, the tip is directly

detecting electroactive species which are generated at the sample surface without addition of a synthetic redox mediator. The substrate generation / tip collection mode can be used for monitoring enzymatic reactions, corrosion, and other heterogeneous processes at the substrate surface.

Iron is a required nutrient by most living organisms. The biogeochemical cycling of iron alternates between soluble ferrous iron (Fe^{2+}), insoluble ferrous iron (FeS_2) and insoluble ferric iron (FeOOH, Fe_2O_3). Dissimilatory Fe(III) reduction is an anaerobic respiratory process carried out by microorganisms to oxidize organic carbon in soils and sediments. Hence, it plays a significant role in global carbon cycling. Fe(III) reducing bacteria utilize Fe(III) as a terminal electron acceptor during this process. Dissimilatory Fe(III) reduction is central to the biogeochemical cycling of Fe, Mn, and other trace elements (Lovely, 1991; Lovley, Coates, Saffarini, & Lonergan, 1997).

Compared to the wealth of knowledge existing on the molecular details of aerobic respiration, denitrification, and sulfate reduction, the molecular mechanism of Fe(III) reduction is poorly understood. It has been hypothesized that iron reducing bacteria must physically contact the Fe(III) oxide surface before reduction occurs. Alternatively, the bacteria may excrete electron shuttles that subsequently reduce Fe(III) without physical contact required. Fe^{2+} is the end result of Fe(III) respiration by the bacteria and can be detected electrochemically with amalgam electrodes (Brendel & Luther, 1995; Taillefert, Luther, & Nuzzio, 2000). Although Fe(III) reducing proteins have been isolated from several bacteria, a Fe(III) terminal reductase enzyme has only recently been definitively identified by DiChristina et al. (DiChristina, Moore, & Haller, 2002). The present thesis strives to determine whether Fe(III) reductase is catalyzing the reduction of Fe(III)

containing minerals. For this purpose, Au/Hg and Pt/Hg amalgam electrodes were combined with SECM imaging for detecting Fe^{2+} production at the solid-liquid interface.

The development and optimization of SECM imaging with amalgam microelectrodes for the investigation of chemical processes occurring at the interface between microorganisms and Fe(III) containing mineral surfaces is presented. This new approach will provide topographical and electrochemical information on respiratory processes involving heavy metal ions at the micrometer scale. The amalgam microelectrodes permit measurement of localized biological and chemical surface processes involving species with negative reduction potentials. Topographical and chemical information can now be obtained, which is critical to the investigation of complex biosystems and biological processes.

1.2 Goals of this Thesis

The complex interactions between chemical processes and biological activity at the microbe-mineral interface motivate the analytical research presented in this thesis. *In-situ* analytical techniques such as SECM can be adapted and optimized to investigate biogeochemical processes with high spatial and temporal resolution. The main goal of this thesis was the development and optimization of SECM imaging with amalgam microelectrodes, and their application for imaging chemical and biochemical processes at microbe-mineral interfaces. This lead to three work packages investigated in the course of this study.

(1) In chapter 4.1, the development and fabrication of Au/Hg microelectrodes with a diameter of 25 μm and their application for SECM imaging of Mn^{2+} dissolution

from a microstructured $MnCO_3$ (rhodochrosite) surface is discussed. In order to obtain quantitative data on the Mn^{2+} evolution at mildly acidic conditions, square wave voltammetry techniques were applied. The application of gold/mercury (Au/Hg) amalgam UMEs in SECM imaging experiments has been demonstrated for the first time in this study (Rudolph, et al., 2004). The investigation of manganese and iron reduction at microbe-mineral interfaces is the ultimate objective of this research.

(2) Chapter 4.2 investigates the oxidative degradation of ZnSe waveguides applied in IR spectroscopy and optical IR evanescent field sensing. The investigation of the corrosion resistance of DLC protected ZnSe waveguides vs. uncoated crystals exposed to strongly oxidizing hydrogen peroxide solutions is of significant interest for a more widespread applicability of this novel technology. SECM imaging in combination with square wave anodic stripping voltammetry utilizing amalgam microelectrodes has been applied in this study.

The electrochemical determination of Zn^{2+} formation using scanning amalgam microelectrodes has been correlated with the onset of corrosion at DLC layer defects at protected ZnSe waveguide surfaces. Concentration profiles and laterally resolved information was obtained by combining SECM and anodic stripping voltammetry at scanning amalgam microelectrodes. In addition to detailed information on the ZnSe corrosion processes, this study confirms the utility of diamond-like carbon layers as highly protective IR-transparent coating for optical waveguides (Janotta et al., 2004).

(3) In chapter 4.3, we report a novel application of SECM using Pt/Hg microelectrodes as a powerful analytical tool for *in-situ* read out of the redox activity of redox proteins or redox protein complexes involved in metal reduction. In this study, the

detection of the protein catalyzed reduction of Fe^{3+} above active protein complexes separated in native 2D gels is demonstrated for the first time (Rudolph, et al., 2005).

2. BACKGROUND

2.1 SECM with Amalgam Microelectrodes

Trace metals of environmental relevance are primarily detected by voltammetric techniques (Desmond et al., 1998; M.-L. Tercier, Buffle, & Graziottin, 1998; Taillefert et al., 2000). Electrochemical detection schemes for trace metal analysis have been established utilizing hanging mercury-drop electrodes and thin film mercury electrodes (Seelig & Blount, 1979; Barbeira & Stradiotto, 1997). Iridium, gold, silver, platinum, and carbon fiber based mercury amalgam ultramicroelectrodes (UMEs) have been developed for electroanalysis of trace metals and sulfides (Wechter & Osteryoung, 1989; Nyholm & Wikmark, 1993; Brendel & Luther, 1995; M. L. Tercier, Parthasarathy, & Buffle, 1995; K. Xu, 1997). Ultramicroelectrodes (UME) offer advantages over macroelectrodes such as higher sensitivity, decreased double-layer capacitance, and lower ohmic losses.

Brendel and Luther developed Au/Hg amalgam microelectrodes (diameter 50-100 μm) for the determination of dissolved Fe^{2+}, Mn^{2+}, O_2, and H_2S using linear sweep and square wave voltammetry in porewaters of marine and freshwater sediments (Brendel & Luther, 1995; K. Xu, 1997). Square wave voltammetry (SWV) is primarily used for these measurements because of its sensitivity and rejection of background current enabling enhanced signal-to-noise ratios. The potential window of Au/Hg amalgam UMEs is limited by the oxidation of mercury at positive potentials and the high overpotential for hydrogen evolution at negative potentials and enables direct (i.e. no preconcentration) detection of species with negative reduction potentials including Mn^{2+}, Fe^{2+}, and O_2.

Scanning electrochemical microscopy (SECM) is a scanning probe technique, which provides information on the (electro)chemical activity at sample surfaces at the microscale. In the late 1980's, Bard et al. and Engstrom et al. established the fundamental principles of SECM (Engstrom, Weber, Wunder, Burgess, & Winquist, 1986; Liu, Fan, Lin, & Bard, 1986). SECM provides the unique capability to perform a wide variety of electroanalytical measurements with high spatial resolution in close proximity to a sample surface (Mirkin & Horrocks, 2000). In a typical SECM experiment, the UME tip scans at a constant height across a sample surface providing electrochemical information at the solid-liquid and liquid-liquid interfaces. Disk microelectrodes are commonly utilized for SECM, however, conical, ring, and sphere cap electrodes of various geometries have also been applied in SECM experiments (Mirkin, Fan, & Bard, 1992; Lee, Amemiya, & Bard, 2001; Liljeroth, Johans, Slevin, Quinn, & Kontturi, 2002).

A general theory for sphere cap microelectrodes used in SECM experiment has been established by the groups of Daniele and Denuault (Fulian, Fisher, & Denuault, 1999; Selzer & Mandler, 2000; Daniele, Bragato, Ciani, & Baldo, 2003). Experimental data on the approach behavior of sphere cap mercury-coated platinum microelectrodes during SECM experiments was published by Daniele and co-workers, with current/distance curves recorded above insulating substrates for the determination of heavy metals (Ciani, Daniele, Bragato, & Baldo, 2003). The principle advantage of Hg amalgam UMEs is their capability to monitor reduction-oxidation (redox) processes of heavy metal ions in an imaging mode when applied during SECM experiments. Microscale insight on biogeochemical processes involving redox sensitive species such as

Mn^{2+} at mineral-water interfaces is now feasible via SECM-based investigations with Hg amalgam UMEs.

2.2 Biogeochemically Relevant Redox Processes

The *in-situ* detection of chemical species such as Mn^{2+} and Fe^{2+} is attracting increasing interest for understanding the bioavailability of dissolved species during environmental and geological chemical reactions at the microbe-mineral interface (Brendel & Luther, 1995; M. L. Tercier et al., 1995; Daniele, Bragato, Baldo, Wang, & Lu, 2000). It has been noted by geologists that Mn^{2+} plays a major role in suboxic sediments and early diagenetic reactions (Calvert & Price, 1972; C. R. Myers & Nealson, 1988).

A significant source of Mn^{2+} and Fe^{2+} in marine sediments results from microbial reductive dissolution of manganese and iron oxides during anaerobic respiration of natural organic matter (Froelich et al., 1979; Lovely, 1991; Thamdrup, Rossello-Mora, & Amann, 2000). The presence or absence of Mn^{2+} and Fe^{2+} plays an important role in these geological processes, however, the underlying mechanisms of bacterially-mediated dissimilatory iron and manganese reduction remains poorly understood (Arnold, DiChristina, & Hoffmann, 1988; Newman & Kolter, 2000; J. M. Myers & Myers, 2001; DiChristina et al., 2002). As another example, the mechanisms of formation and dissolution of sulfide minerals is also not well understood, even though these minerals play a significant role in geological processes (Berner & Petsch, 1998). Iron and manganese are involved in complex microbially-mediated metal cycles associated with biofilms in corrosion processes (K. Xu, 1997). These natural biofilms accumulate

significant amounts of manganese and iron oxides, and hydroxides via bacterial oxidation (Ghiorse, 1988). Laterally resolved investigations of chemical dissolution and precipitation processes at the microscale are needed to probe and determine the reaction mechanisms involved in microbial or chemical metal cycling in natural environments such as marine sediment.

2.3 Corrosion Studies with SECM

A variety of surface analysis tools have been used to study corrosion processes at materials such as steel, brass and glass (Marcus, Maurice, Costa, & Galtayries, 2002). *In-situ* and *ex-situ* scanning probe techniques including atomic force microscopy (AFM) and scanning tunneling microscopy (STM) have been applied to study changes in surface morphology and corrosion processes (Schreyer, Suter, Eng, & Bohni, 1998; de Wit, 2001; Maurice, Klein, & Marcus, 2002; Kleber & Schreiner, 2003). Electrochemical methods have extensively been applied, in particular, to characterize the corrosion resistance and barrier properties of protective coatings. Analytical techniques such as scanning electrochemical microscopy (SECM) are of substantial interest for *in-situ* electrochemical investigations as they enable insight on localized corrosion events (Still & Wipf, 1997; Katemann et al., 2003; Lister & Pinhero, 2003).

SECM is among the preferred techniques for corrosion studies for a variety of reasons. In comparison to STM, there is no limitation based on the conductivity of the sample, as SECM works for both, insulating and conducting surfaces. Furthermore, structural surface effects can be correlated with localized electrochemical activity in SECM. The UME can be used to either initiate the reaction and/or electroactive

corrosion products can be detected at the UME. The current measured at the UME provides quantitative information on the involved electrochemically active corrosion processes. Corrosion investigations with SECM have been performed at the surface of several metals including steel, Al, Ni, Ti, and at semiconductors (Wipf, 1994; Horrocks, Mirkin, & Bard, 1994; Basame & White, 1995; Paik, White, & Alkire, 2000; Paik & Alkire, 2001; Lister & Pinhero, 2003). Furthermore, SECM is a powerful tool for investigating the dissolution characteristics of electrically insulating materials, such as e.g. ionic single crystal surfaces (Macpherson, Unwin, Hillier, & Bard, 1996).

2.4 Determination of Redox Protein Activity

Microbial metal respiration plays a key role in a wide variety of environmentally relevant processes, including the biogeochemical cycling of metals, trace elements, and phosphate as well as the degradation of natural and contaminant organic matter (Lovely, 1991). The bioavailability and *in-situ* detection of dissolved chemical species such as Fe^{2+}, Fe^{3+}, and $S_2O_3^{2-}$ is attracting increasing interest for understanding the environmental and geological chemical reactions at the microbe-mineral interface (Brendel & Luther, 1995; M. L. Tercier et al., 1995; Daniele et al., 2000). Microbial reductive dissolution of iron oxides is a significant source of Fe^{2+} during anaerobic respiration of natural organic matter in marine sediment (Froelich et al., 1979; Lovely, 1991; Thamdrup et al., 2000).

A variety of bacteria such as *Shewanella* and *Geobacter* are responsible for dissimilatory metal-reduction have been extensively studied (C. R. Myers & Myers, 1992; Lloyd, Sole, Van Praagh, & Lovley, 2000). However, the mechanisms by which these bacteria reduce metals, especially Fe(III) and Mn(III, IV) oxides, remain largely

unclear. Recent research focuses on mechanisms involving direct contact of the microbe with the mineral surface, or via electron shuttles using humic acids, quinones, or c-type cytochromes (Arnold et al., 1988; Newman & Kolter, 2000; J. M. Myers & Myers, 2001; DiChristina et al., 2002). Multi-heme cytochrome complexes have been determined to be localized at the outer membrane of *Shewanella putrefaciens*, and to be key components of bacterially-mediated dissimilatory Fe^{3+} and Mn^{4+} reduction (C. R. Myers & Myers, 1992).

Single-stage matrix-assisted laser desorption ionization time-of-flight (MALDI-TOF) mass spectrometry and peptide mass fingerprinting of tryptic digests of individual proteins within a respiratory Fe(III) reductase complex indicate that the complex contains a near complete complement of assimilatory sulfate reduction proteins. These findings suggest that Fe(III) respiring bacteria have evolved a dissimilatory Fe(III) reduction system based on assimilatory sulfate reduction principles, and that the "enzymatic" Fe(III) reduction pathway actually terminates with the purely chemical (abiotic) reduction of Fe(III) by enzymatically-produced sulfur compounds (DiChristina, unpublished results). However, the molecular mechanism of anaerobic microbial metal respiration is still poorly understood, and the metal reductase proteins or protein complexes involved in the electron transfer to the metals have yet to be unambiguously identified. Hence, our focus in this field is directed to identify proteins or protein complexes involved in anaerobic respiratory metal reduction.

Leang et al. (2003) and Beliaev & Saffarini (1998) have demonstrated that a multi-heme c-type cytochrome, which is localized at the outer membrane of metal reducing microbes *Shewanella oneidensis* and *S. putrefaciens*, is essential for electron

transport to the terminal electron acceptor (Fe(III) and Mn(IV)). Electron transport to the outer membrane is a key feature of the metal reduction mechanism. Hence, an important question to answer is whether direct contact of microbial cells with metal oxides or terminal electron acceptors is required for the reduction to occur.

Blue native (BN)- and colorless native (CN)- polyacrylamide gel electrophoresis (PAGE) are generally used to isolate catalytically active, multi-protein complexes of respiratory chains (Schaegger & Von Jagow, 1991; Schaegger, Cramer, & von Jagow, 1994). Although this technique is widely used, it does not provide direct information on catalytic activities. Furthermore, only few staining reagents for many of these proteins and protein complexes are available. Two-dimensional (2D) gel electrophoresis coupled with mass spectrometry has been used to determine the relative abundance of microbial cellular proteins. A disadvantage of this technique is through that the denaturation can disrupt the protein function. In the present thesis, a direct electrochemical detection scheme for the redox activity of respiratory proteins and protein complexes after separation but still within 2D gels is introduced for rapid stain-free identification of active protein bands via SECM with amalgam microelectrodes.

3. EXPERIMENTAL

3.1 Instrumentation

Voltammetric experiments were conducted using an electrochemical workstation (CH 660, CH Instruments, Austin, TX) equipped with an electrochemical cell in a three-electrode configuration comprising a saturated calomel reference electrode (SCE), a Pt counter electrode, and an amalgam (Au/Hg or Pt/Hg) working UME. All measurements were performed in a Faraday cage. A three-electrode configuration with an Ag/AgCl reference electrode and a Pt counter electrode was used for SECM line scans and imaging. The micropositioning system (SPI Scientific Precision Instruments, Oppenheim, FRG) and bi-potentiostat (PG100, IPS-Jaissle, Waiblingen, FRG) of the SECM are controlled by a PC via an A/D-D/A board (DAS1602-16, Plug-In-Electronic, Eichenau, FRG). G. Wittstock (University Oldenburg, FRG) provided the software ("Mira") controlling the positioning system and the data acquisition. Observation of the microelectrode during positioning and scanning was enabled by a CCD camera positioned underneath the transparent sample. The software package "Mira" and data analysis/visualization software (IDL, Creaso, Munich, FRG) was used for SECM data evaluation.

3.2 Microelectrode fabrication

Au/Hg amalgam microelectrodes have been fabricated by melting a 25 μm Au wire (Goodfellow, Berwyn, PA) into a 1 mm soda lime glass capillary (Hilgenberg GmbH, Malsfeld, FRG). Pt/Hg amalgam microelectrodes have been fabricated by melting a 25 μm Pt wire (Goodfellow, Berwyn, PA) into a 1 mm borosilicate glass capillary (Hilgenberg GmbH, Malsfeld, FRG). The disk-shaped microelectrode was exposed through grinding. An additional grinding step at a 30° angle results in a conical shape of the glass insulation around the exposed wire. The microelectrode was polished with aluminium (grain size: 6 and 3 μm) and diamond (grain size: 1 and 0.5 μm) slurries, respectively, on a polishing microcloth. The electrodes were sonicated in deionized water for 10 minutes after polishing. The microwire was contacted with silver epoxy (Epo-Tek H2OE, Polytek, Waldbronn, FRG) to a copper wire (diameter 0.5 mm) and dried at 60°C for 24 h. The effective electrode radius of the exposed microdisk was electrochemically determined by recording cyclic voltammograms in 10 mM $Ru(NH_3)_6^{3+}$ solution with 0.5 M KCl as supporting electrolyte.

3.3 Amalgam Plating

Electrodeposition of liquid mercury onto the gold and platinum disk UMEs was performed potentiostatically at -0.1 V vs. SCE from 10 mM $Hg_2(NO_3)_2$ solution at pH 1 (acidified with nitric acid). Subsequently, the amalgams were stored in deionized water. The amount of mercury plated onto the microelectrodes was determined by using equation 2 (Colyer, Luscombe, & Oldham, 1990).

$$V = QM / F\rho_0 = \pi h(3a^2 + h^2) / 6 \qquad (2)$$

In equation 2, a is the radius of the microelectrode, h is the height of the mercury deposit, Q is the charge, and M and ρ are the atomic mass and density of mercury, respectively. The volume of mercury deposited at the UME was confirmed from the oxidization of the deposited mercury using linear sweep voltammetry (-0.3 to 0.3 V) in 1 M KSCN at a scan rate of 10 mV s^{-1} after measurements.

When compared to Ir/Hg or Pt/Hg amalgam electrodes, the geometry of Au/Hg amalgam electrodes is frequently described as less reproducible due to the high solubility of gold in mercury (Vydra & et al., 1976). It has been shown, however, that the sensitivity of Au/Hg UMEs, and the reproducibility of the response markedly increases after a conditioning step (Brendel & Luther, 1995). In order to maintain the integrity of the electrode surface, a potential of -9 V is applied to the Au/Hg amalgam electrode which removes any mercuric oxides, which may have formed during the plating process (Stojek & Kublik, 1975). A plating time of 70 s and a conditioning period of 30 s were applied for gold electrodes with a diameter of 25 μm, following thorough optimization. Resulting, reproducible and durable gold amalgam microelectrodes have been fabricated.

3.4 Amalgam Microelectrode Characterization

Derived from the approach of Brendel and Luther (Brendel & Luther, 1995), the fabrication of Au/Hg and Pt/Hg amalgam microelectrodes with a diameter of 25 μm was developed and optimized. In principle, amalgam microelectrodes are formed by electrodeposition applying potentiostatic conditions. The geometry of Au/Hg amalgam electrodes is frequently described as less reproducible when compared to Pt/Hg amalgam electrodes, due to the high solubility of gold in mercury (Vydra & et al., 1976).

However, it has been shown that the sensitivity of Au/Hg microelectrodes and the reproducibility of their response markedly increases after a conditioning step (Stojek & Kublik, 1975). A potential of -9 V is applied to the Au/Hg amalgam electrode resulting in increased integrity of the electrode surface by removing any mercuric oxides, which may have formed during the plating process.

We have investigated the behavior and lifetime of Au/Hg vs. Pt/Hg amalgam electrodes in more depth by monitoring the calibrations of the electrodes over a nine day period. The Au and Pt amalgam microelectrodes were calibrated using anodic stripping square wave voltammetry (-1.6 V to -0.2 V; frequency = 40 Hz; scan rate = 50 mV s^{-1}) by standard addition of 25 μL of 40 mM $MnCl_2$, and 25 μL of 40 mM $ZnCl_2$ in deaerated deionized water (Figure 2 & 3). The peak definition for Mn^{2+} and Zn^{2+} detection at the Au/Hg electrode greatly decreases over the nine day period (Figure 2(a) and (b)). The peak definition for Mn^{2+} and Zn^{2+} detection at the Pt/Hg electrode on the ninth day of usage, however, is comparable to detection on its first day of use (Figure 3(a) and (b)). Stripping of manganese and zinc provides a linear relationship between concentration and current within the concentration range of 50 to 500 μM. The calibration curves for the two representative microelectrodes on the first and last day of usage are shown in Figure 4. The gold amalgam increases in sensitivity over the course of the experiment. The platinum amalgam increases only marginally over the nine day period. The reproducibility of the calibration measurements is poor on the last measurement day, with the platinum amalgam providing superior reproducibility.

(a)

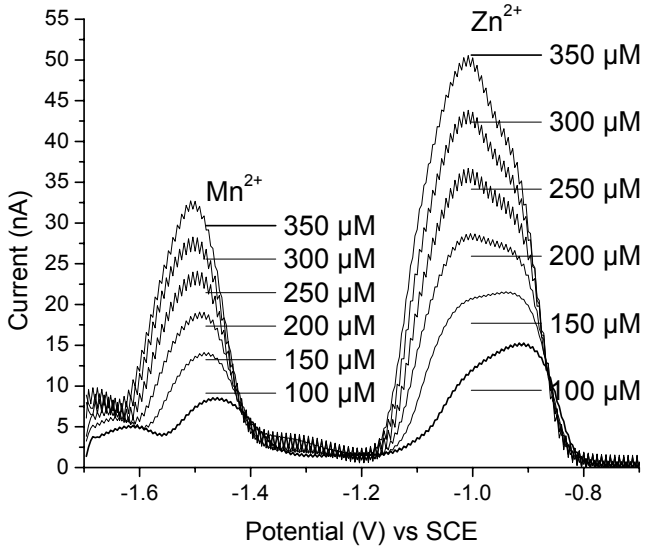

(b)

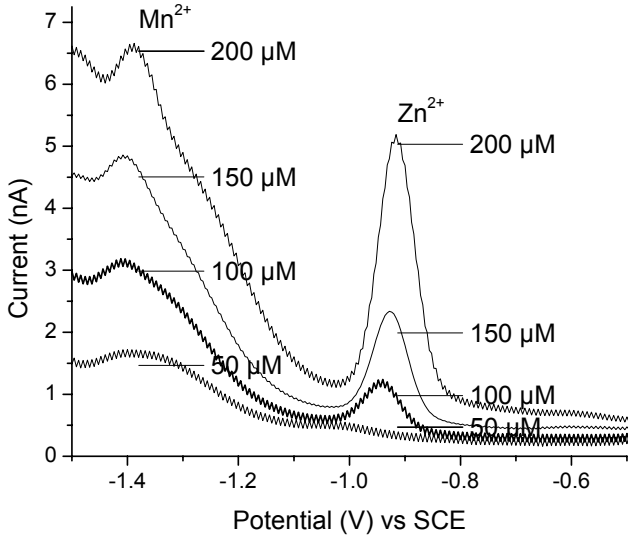

Figure 2: Square-wave voltammograms obtained from Au/Hg microelectrode D2 calibrated for Mn^{2+} and Zn^{2+} in 20 mL deionized water with standard addition of 25 µL of a 40 mM $MnCl_2$ and $ZnCl_2$ stock solutions. (a) Measurement day 1. (b) Measurement day 9.

(a)

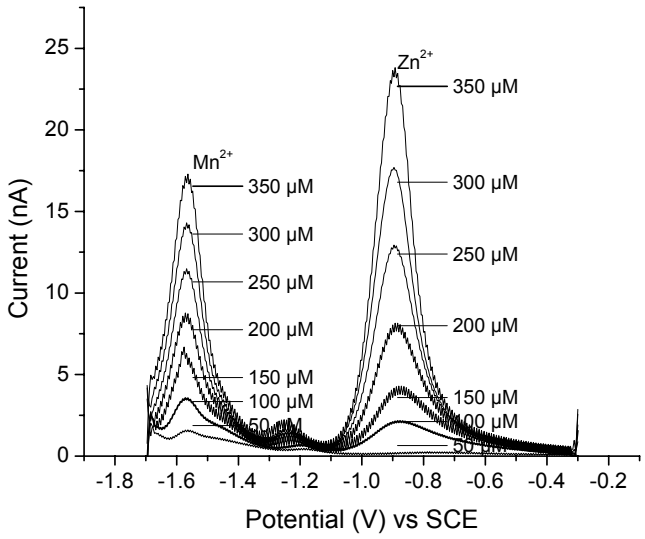

(b)

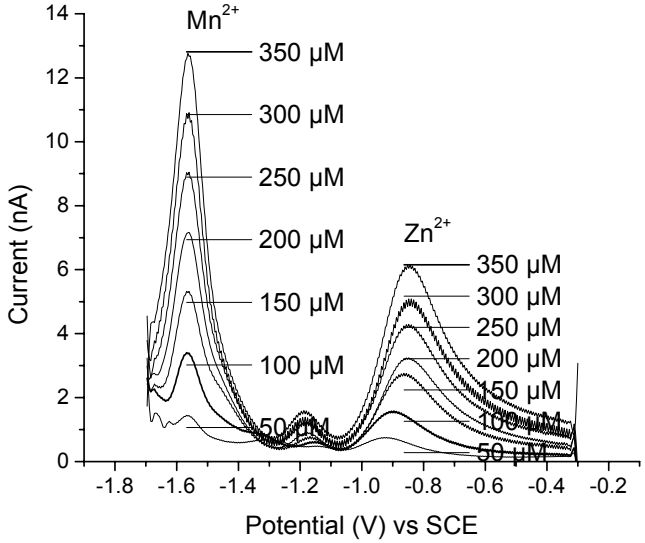

Figure 3: Square-wave voltammograms obtained from Pt/Hg microelectrode R2 calibrated for Mn^{2+} and Zn^{2+} in 20 mL deionized water with standard addition of 25 µL of a 40 mM $MnCl_2$ and $ZnCl_2$ stock solutions. (a) Measurement day 1. (b) Measurement day 9.

(a) (b)

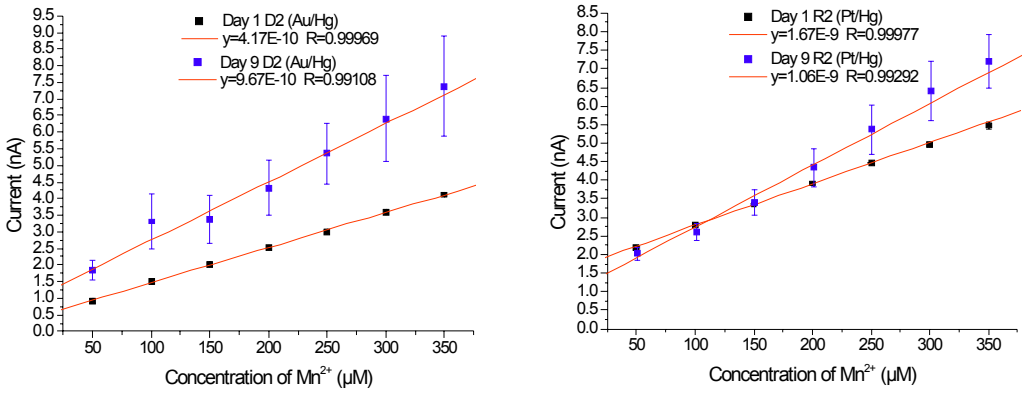

Figure 4: Mn^{2+} calibration curves for Au/Hg and Pt/Hg microelectrodes. (a) Au/Hg calibration curve comparison between first and last measurement day. (b) Pt/Hg calibration curve comparison between first and last measurement day. Note that error bars at lower concentrations are smaller than the symbol size.

The limit of detection (LOD) was determined for each electrode from the slope of the calibration functions and the standard deviation of blank measurements (deionized water). Table 1 gives the LOD for each amalgam microelectrode as the electrode ages with time. The LOD for the Au/Hg amalgam microelectrode is nearly two times that of the Pt/Hg amalgam microelectrode on the initial measurement day. The LOD of the Au/Hg microelectrode actually decreases over the course of the nine days yet also shows decreased reproducibility. When electrodes are compared, the Pt/Hg amalgam in general performed better over the course of the experiments. The overall LOD for the Pt amalgam microelectrode is much lower initially while it retains higher reproducibility throughout the nine day lifetime. The trends presented here are representative of Au/Hg and Pt/Hg amalgam microelectrodes for eight tested electrodes.

Table 1: An Au/Hg microelectrode is compared with a Pt/Hg microelectrode in regards to the limit of detection (LOD) for each microelectrode on the respective day of measurement.

Electrode	Day	LOD	Electrode	Day	LOD
D2 (Au/Hg)	1	32.00 µM +/- 5.93	R2 (Pt/Hg)	1	16.21 µM +/- 0.33
D2 (Au/Hg)	5	26.36 µM +/- 7.69	R2 (Pt/Hg)	5	15.61 µM +/- 1.08
D2 (Au/Hg)	9	25.85 µM +/- 14.7	R2 (Pt/Hg)	9	26.5 µM +/- 5.08

3.5 Square Wave Voltammetry

In square-wave voltammetry, the potential is ramped as a function of time utilizing a square modulation of the forward (positive) and reverse (negative) potential pulses (Figure 5) (K. Xu, 1997). The current is measured at the end of each pulse. The difference between the forward and reverse pulse (resultant current) are square wave voltammograms. Voltammograms can be scanned anodically (-1.6 to -0.1 V) and cathodically (-0.1 to -1.6 V) depending on the chemical species of interest and their characteristic redox potential window.

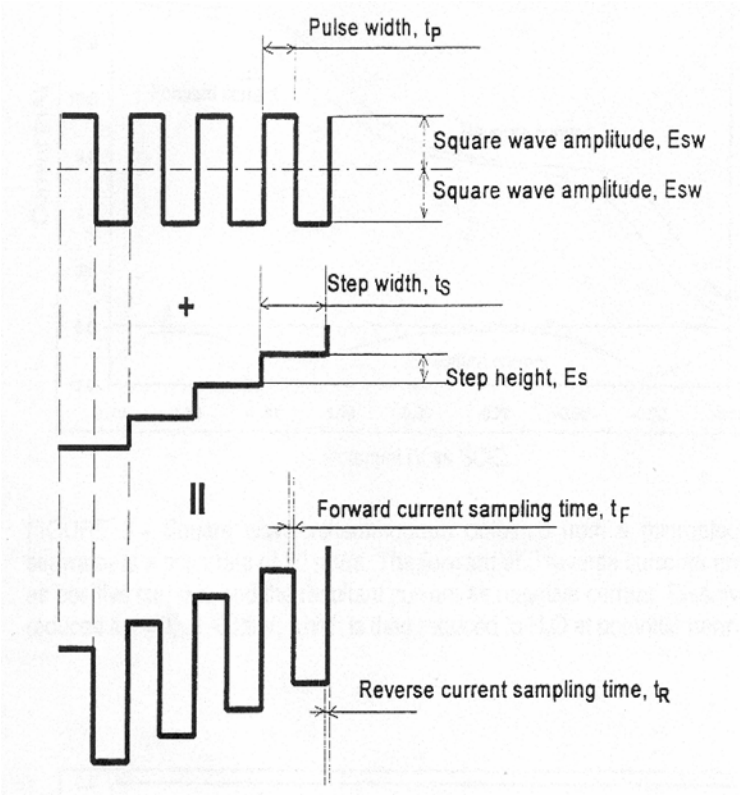

Figure 5: The waveform of square wave voltammetry is the sum of a symmetrical square wave and a staircase wave of the same phase and frequency.

Throughout this thesis, the positive scan direction is the anodic scan and the negative scan direction is the cathodic scan (Figure 6). The entire voltammetric scan is completed in less than 20 seconds at the selected SWV parameters (-1.6 V to -0.1 V; scan rate: 50 mVs^{-1}; frequency: 40 Hz; amplitude: 15mV).

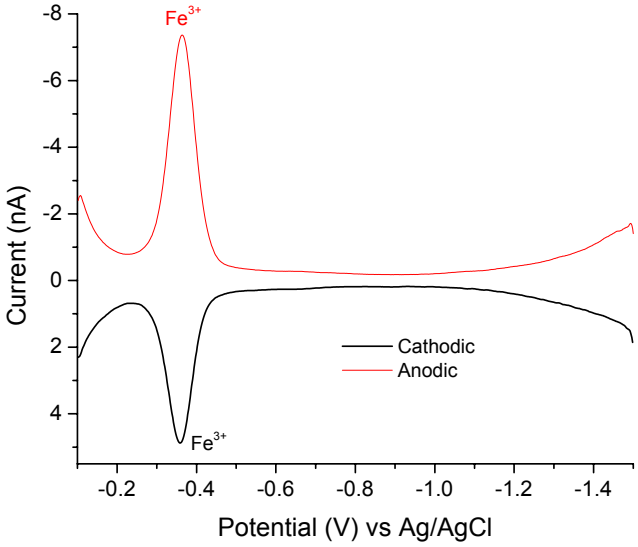

Figure 6: Example of an anodic and cathodic square wave voltammogram recorded at a Pt/Hg amalgam microelectrode in bulk solution containing 300 µM ferric citrate. SWV parameters: -1.6 V to -0.1 V; scan rate: 50 mVs^{-1}; frequency: 40 Hz; amplitude: 15 mV.

3.6 Sample Preparation

3.6.1 $MnCO_3$ Samples

$MnCO_3$ microstructures were prepared by precipitating a mixture of 2.5 M $MnCl_2$ and 0.025 M $NaHCO_3$ twice onto a microscope glass slide (Johnson, 1982). The glass plate was rinsed with deionized water between precipitations to dissolve co-precipitated NaCl and remove non-adhesive crystallites. The sample was microstructured by removing some of the rhodochrosite precipitate with a sharp pipette tip thus creating microstructures of manganese carbonate spots with an average size of 100-200 µm at the surface of the glass slide (Figure 8). A surface profilometer (Sloan Dektak 3ST, Veeco, Sunnyvale, CA) was used to determine the height of the precipitate. A uniform thickness

of 1.2 μm was recorded by profilometer measurements of the rhodochrosite precipitate. The exact size of each spot was determined using a calibrated CCD camera (T.I.M.M SPI Scientific Precision Instruments, Oppenheim, FRG) prior to the SECM experiments. Acidification with acetic acid, formic acid, or hydrochloric acid ensured controlled dissolution of $MnCO_3$.

A schematic representation of the experimental set-up for imaging the dissolution of $MnCO_3$ spots is given in Figure 7.

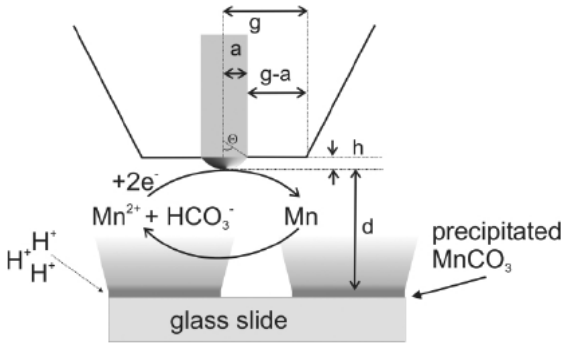

Figure 7: Schematic diagram of an Au/Hg UME approaching a mineral substrate (i.e. $MnCO_3$) that dissolves in mildly acidic conditions. Mn^{2+} is detected in generation/collection mode at the Au/Hg UME positioned at an optimum distance (d) to the substrate, thus maximizing the electrode response. (d = distance from substrate, h = mercury sphere cap height, a = electrode radius, g = glass sheath radius).

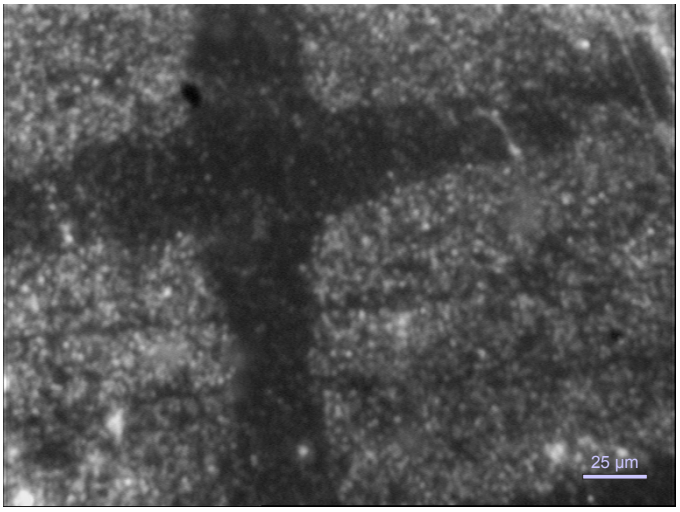

Figure 8: Optical image of microstructures of manganese carbonate with an average spot size of 100-200 µm at the surface of a glass slide.

To electrochemically measure the dissolution of rhodochrosite in two dimensions, it is necessary to ensure reproducible dissolution rates during SECM imaging. The composition and concentration of the acidic buffer used to maintain constant production of Mn^{2+} was optimized in bulk experiments by electrochemically measuring the production of Mn^{2+} as a function of time using anodic square wave voltammetry (Figure 9).

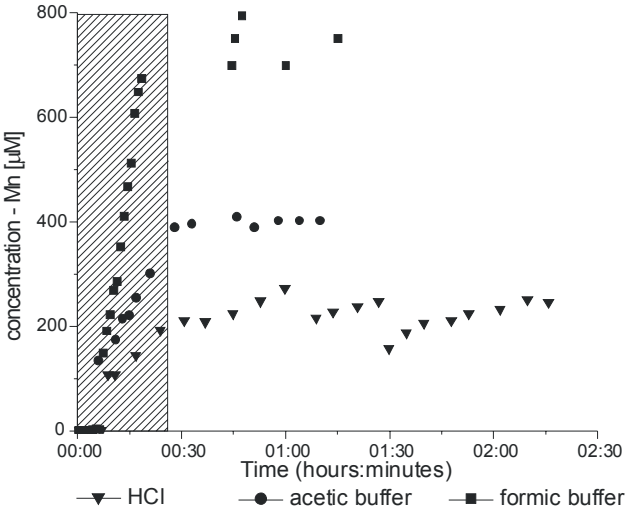

Figure 9: The dissolution behaviour of rhodochrosite at different pH as a function of time was triggered by hydrochlorid acid, formate buffer and acetate buffer. The production of Mn^{2+} was measured at an Au/Hg microelectrode by square wave voltammetry in the presence of: (a) 0.125 mM hydrochloric acid (pH 3.9); (b) a 0.05 M acetic acid/0.5 M sodium acetate solution (pH = 4); and (c) a 0.07 M formic acid/0.7 M sodium formate solution (pH 4). The shaded area shows the dissolution rates of Mn^{2+} within a period of 30 min, which is the time required for SECM measurements.

The pH was optimized to achieve linear sample dissolution rates in the period of 10-30 min, which is relevant to the time scale of SECM imaging. It was found that a pH of 4 is low enough to ensure constant dissolution during that time period. Constant dissolution rates throughout the SECM measurements were ensured by adjusting the buffer capacity. Three different acidic solutions were tested including two buffer systems. Addition of 0.125 mM hydrochloric acid (pH = 3.9), acetate buffer (0.05 M acetic acid in 0.5 M acetate solution; pH = 4) and formate buffer (0.07 M formic acid in 0.7 M formate solution; pH = 4) resulted in dissolution of the $MnCO_3$ substrate according to

$$MnCO_3 + H^+ \rightarrow Mn^{2+} + HCO_3^-$$

The production of Mn^{2+} was linear up to a concentration range exceeding 600 μM in formate buffer, however, not in hydrochloric acid and acetate buffer (Figure 9). The duration of the SECM measurements should not exceed a period of 30 min to ensure constant dissolution rates of rhodochrosite indicated by the shaded area in Figure 9. SECM experiments were performed in formate buffer (pH 4) at concentrations well within the linear calibration range of the Au/Hg UME (Figure 11(b)).

3.6.2 ZnSe/DLC Waveguides

The DLC coatings were deposited at the surface of ZnSe ATR elements (50*20*2 mm, 45°, Macrooptica Ltd., Moscow, Russia) by pulsed laser desorption physical vapor deposition at Joanneum Research, Niklasdorf, Austria. An electro-graphite target (99.5 % carbon, impurities of vanadium, titanium, hydrogen and oxygen) was used for the ablation of carbon via pulsed Nd:YAG laser irradiation at a wavelength of 1064 nm. The pulse energy was 1 J with a pulse duration of 10 ns at a repetition rate of 10 Hz. The emitted species were deposited at room temperature (approx. 25 °C) in argon atmosphere. A detailed description of the DLC film preparation is given by (Lackner et al., 2003).

3.6.3 Native Gels

The protein complexes from *Shewanella oneidensis* were isolated and separated by 2-D native gel electrophoresis (DiChristina, unpublished results). One gel was stained for Fe (III) activity and then positioned in parallel with the unstained gel in order to electrochemically determine and verify the active protein band zone. After separation, the active zones of the gels (2.5 x 2.5 cm) containing the reductase protein bands were

mounted in a designated SECM sample cell with a groove corresponding to the dimensions and height of the native gel (Figure 10).

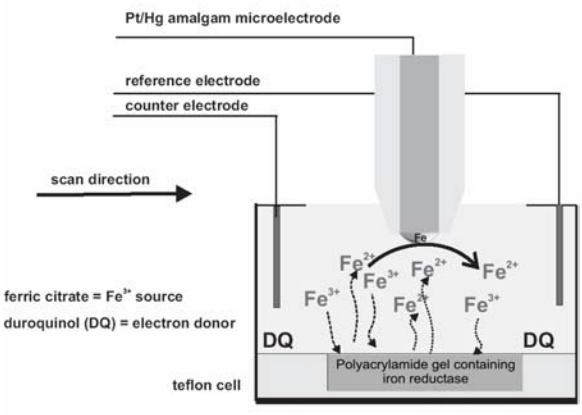

Figure 10: Scheme of the SECM experiment conducted in generation/collection mode combined with stripping voltammetry for the detection of Fe^{3+} reduction catalyzed by a reductase / reductase complex contained in a polyacrylamide gel after electrophoretic separation.

4.1 SECM Imaging of Rhodochrosite Dissolution Using Au Amalgam Microelectrodes

4.1.1 Amalgam Microelectrode Calibration

Individual gold amalgam microelectrodes were calibrated using anodic square wave voltammetry (–1.6 V to –2 V; scan rate: 50 mVs^{-1}; frequency: 40 Hz) by standard addition of 25 µL of 40 mM $MnCl_2$ in deaerated deionized water before and after SECM experiments (Figure 11(a), (b) and (c)). Square wave voltammograms for a series of Mn^{2+} concentrations are shown in Figure 11(a). A linear relationship between peak height and the concentration of Mn^{2+} added to the solution was derived (Figure 11(b)). The relative standard deviations increase towards higher Mn^{2+} concentrations due to an additive error during the incremental addition of 25 µL of a Mn^{2+} solution with a concentration of 40 mM per calibration point. Three square wave measurements are averaged per calibration point.

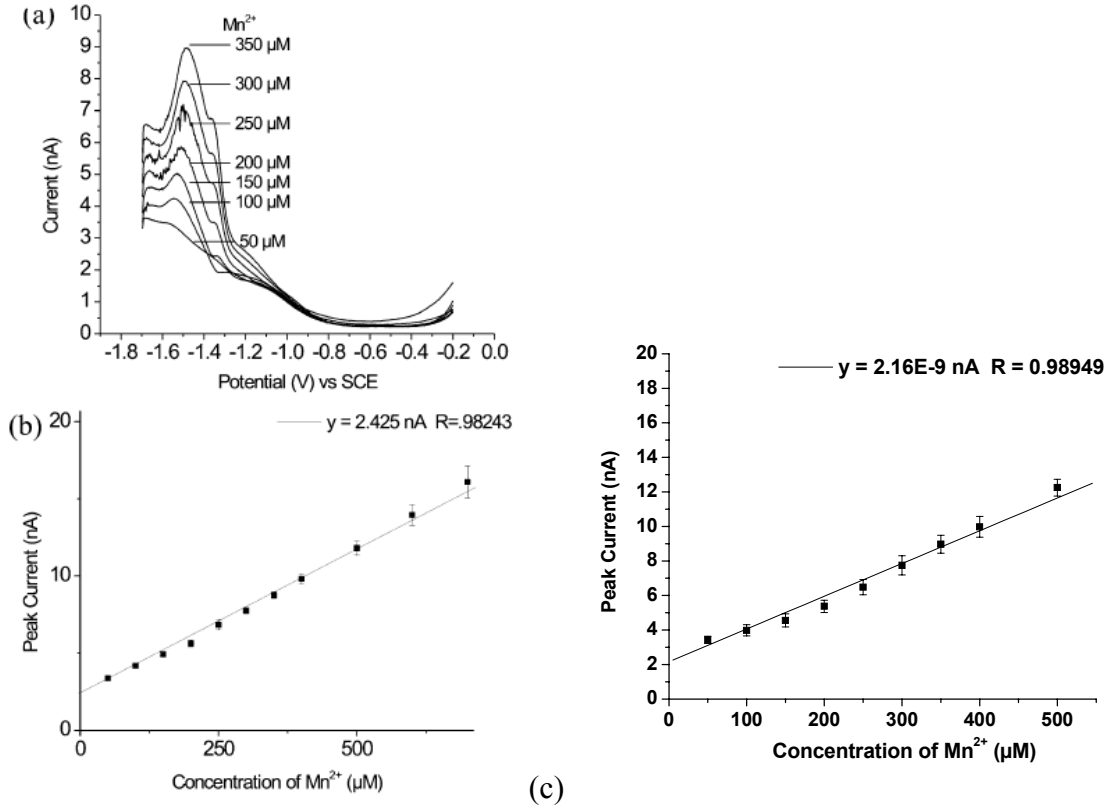

Figure 11: (a) Square-wave voltammograms obtained from microelectrode D4 calibrated for Mn^{2+} in 20 mL deionized water with standard addition of 25 µL of a 40 mM $MnCl_2$ stock solution. Mn^{2+} is reduced to Mn^0 at a potential of –1.55 V. (b) Mn^{2+} calibration curve for microelectrode D4 before experiment. (c) calibration curve after experiment. Note that error bars at lower concentrations are smaller than the symbol size.

4.1.2 SECM Approach Curves

Cyclic voltammetry was applied prior to mercury plating in order to determine the effective radii a of the fabricated gold microelectrodes using equation 1 (Kwak & Bard, 1989; Myland & Oldham, 1990).

$$a = I_{ss} / knFDC \qquad (3)$$

The effective radii determined for the series of gold microelectrodes used in this study are given in Table 2.

Table 2: Effective disk radius a, RG value g/a, volume of mercury plated onto the gold film, and k values for a suite of four different microelectrodes. These parameters are used to characterize each microelectrode before any experiments.

Electrode	Effective disk radius (μm)	RG value	Hg volume (μm^3)*	k
D1	12.05	5	18.12	4.30
D2	12.31	10	15.89	4.08
D3	12.25	5	17.67	4.37
D4	12.2	5	20.64	4.32

*Volume of mercury determined from deposition and equation 1.

In equation (3), I_{ss} represents the steady state limiting current, n is the number of exchanged electrons, F is the Faraday constant, D is the diffusion coefficient (D = 6.0×10^{-6} $cm^2 s^{-1}$ for $[Ru(NH_3)_6]^{3+}$), and C the concentration of the redox active species. k is a factor depending on the geometry of the sphere cap electrode and is a function of the effective electrode radius a and the height of the sphere cap h, with $k = 4$ and $h/a = 0$ for disk electrodes (Saito, 1968).

Approach curves with gold microelectrodes were recorded prior to the mercury plating. Early simulations of the negative SECM feedback effect are based on the assumption that the local concentration at the edge of the insulating shielding is equal to the bulk concentration, which is only valid for RG values $\geq$ 10 (RG value = the ratio of the insulating glass radius g, to the electrode disk radius a (Kwak & Bard, 1989; Mirkin et al., 1992; Bard et al., 1994). The successful application of micro disk electrodes with RG values ranging from 1 to 50, however, has been described in several papers, as well as mathematical simulations for smaller RG values (Shao & Mirkin, 1998; Amphlett & Denuault, 1998; Fulian et al., 1999; Lee et al., 2001). In this study, the RG values were

calculated by recording an approach curve in deionized water with O_2 as the redox active species towards an insulating glass substrate and fitting the experimental approach curve to an analytical approximation obtained for different RG values (Amphlett & Denuault, 1998):

$$\frac{I_{tip}}{I_{tip\infty}} = \frac{1}{k_1 + \frac{k_2}{L} + k_3 \exp\left(\frac{k_4}{L}\right)} \qquad (4)$$

I_{tip} and $I_{tip\,\infty}$ are the current at a given distance and the current in bulk solution, respectively. k_1, k_2, k_3, and k_4 are constants depending on the RG value. L is the height of the electrode above the substrate, d, normalized by the effective radius of the electrode a (L = d/a). The results are summarized in Table 2 including the geometric factor k determined using equation (3) for different Au/Hg microelectrodes (Daniele et al., 2003).

SECM approach curves for sphere cap mercury microelectrodes have been described by Daniele and co-workers (Ciani et al., 2003; Daniele et al., 2003). The geometry influencing the effective diffusion towards the tip of the Au/Hg UME was determined using equations (5) and (6).

$$I_{(L)} = \frac{2}{\sin^2(\theta_0)} \int_0^{\theta_0} (I_{disk}(z)) y dy \qquad (5)$$

$$I_{(L)} = 0.873 + \ln(1 + L^{-1}) - 0.20986 \exp[-(L - 0.1)/0.55032] \qquad (6)$$

$I_{(L)}$ is the tip current normalized by the response in bulk solution at a given height L above the sample surface. θ is the angle between a point on the sphere cap surface and the virtual radius of the mercury sphere with θ_0 representing the maximum value for θ determined by the radius of the disk electrode. $I_{disk}(z)$ is the SECM current function calculated by equation (6) (Selzer & Mandler, 2000).

SECM approach curves of mercury-plated microelectrodes recorded in $Ru(NH_3)_6^{3+}$ solution were compared to theoretical approach curves of UMEs considering a sphere cap geometry (Mirkin et al., 1992). Tilt-free positioning of the mercury microelectrode and ensuring that the sample surface was not touched was accomplished by positioning a CCD camera underneath the transparent sample.

Three amalgam electrodes with RG values of 5, and one electrode with a RG value of 10 were investigated in detail (Table 2). The RG values were derived from fitting approach curves towards an insulating substrate (Figure 12 (a),Table 2) (Amphlett & Denuault, 1998). The experimental approach curves for Au/Hg microelectrodes towards an insulating substrate match very well with fitted theoretical approach curves derived from equation (5), as shown in Figure 12 (b). This model was then used to determine the distance *d* between the sample surface and the amalgam microelectrode for scanning experiments following equation (6).

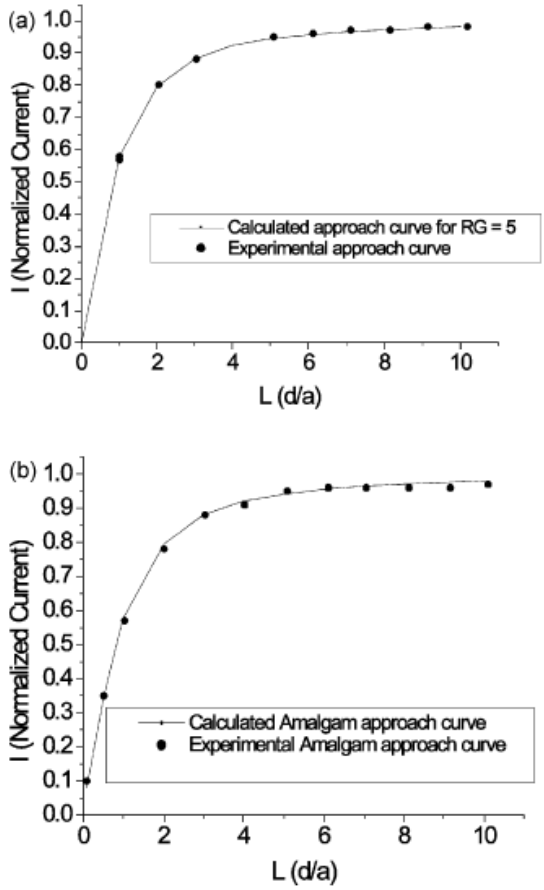

Figure 12: Typical characterization of UMEs in SECM via negative feedback approach curves in 0.5 M KCl using oxygen as a redox mediator. (a) Approach curve of Au disk electrode fitted with theoretical approach curves (equation 4) to calculate RG-values. (b) Approach curve of Au/Hg electrode fitted with theoretical approach curves (equation 5) to calculate θ_0 values for sphere cap disk UMEs.

4.1.3 SECM Imaging of Rhodochrosite Dissolution

Mn^{2+} produced during the dissolution of rhodochrosite is detected in generation/collection mode at the Au/Hg UME. This sample serves as the model system for localized generation of heavy metal ions and laterally resolved detection via scanning amalgam electrodes. In generation/collection mode, the current measured at the UME is inversely proportional to the distance from the source (Fulian et al., 1999). It is thus

necessary to position the UME at an optimum distance *d* from the substrate to maximize the electrode response.

The current obtained during the scan represents a convolution of the Mn^{2+} production and the change in distance between the electrode and the substrate surface due to the geometry of the precipitated rhodochrosite features due to the nature of the constant height measurement. Hence, the topography of the sample has to be recorded in order to obtain quantitative results. Prior to dissolution experiments, the topography of the investigated rhodochrosite feature was determined in feedback mode SECM and compared to profilometry measurements of the sample.

Approach curve experiments were performed in 0.5 M KCl with oxygen as redox mediator above the rhodochrosite substrate in order to determine the optimum scan height (Figure 12 (b)). Once the tip was positioned at a known height determined to be 33 μm, the tip was scanned across the $MnCO_3$ spot in constant height to record its topography (Figure 13).

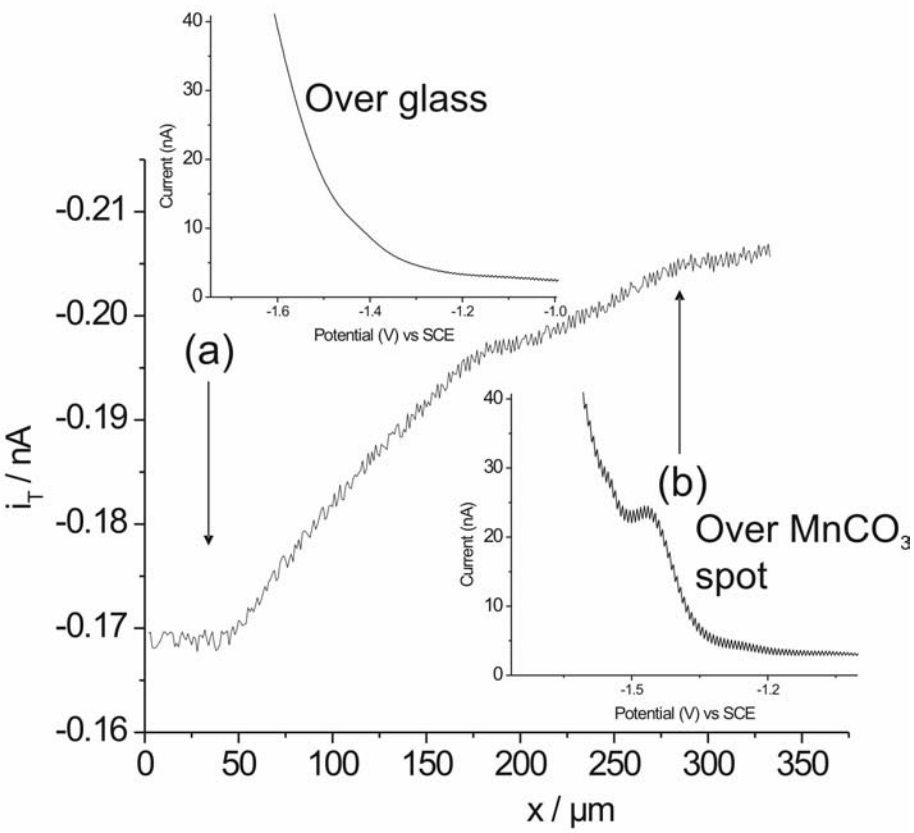

Figure 13: Increase in the amperometric current at –0.5 V in an oxygenated solution as the Au/Hg UME is scanned along the x-axis from the glass (insulating) holder across the dissolving $MnCO_3$ spot at a scan rate of 1 µm s^{-1}. (a) Typical square wave voltammetric measurement at x = 40 µm along the line scan still above the glass slide (scan rate: 50 mV s^{-1}; frequency: 40 Hz). (b) Typical square wave voltammetric measurement at x = 280 µm along the line scan above the $MnCO_3$ spot (scan rate: 50 mV s^{-1}; frequency: 40 Hz). (c) Calculated topography-compensated concentration profile of Mn^{2+} across the dissolving $MnCO_3$ spot measured during a constant height linescan at a distance of 33 µm above the glass surface.

The height above the surface was calculated by fitting the theoretical approach curves to the experimental data following equation 5. The maximum height of the $MnCO_3$ spot was determined to be 1.3 µm based on the negative feedback current obtained during scanning across the sample (Figure 13(c)). The height obtained in the electrochemical

measurement matches well with the profilometer data showing a layer thickness of 1.2 μm measured at the same rhodochrosite precipitate spot prior to the SECM experiments.

The solution was then replaced *in-situ* with formate buffer triggering the dissolution of the microstructured rhodochrosite substrate following the optimization discussed in Section 3.6.1. The Au/Hg UME was scanned at constant height across the dissolving $MnCO_3$ spot and the differential current obtained by square wave voltammetry was recorded during the linescan in generation/collection mode at intervals of 20 μm. Two representative voltammograms at x = 40 μm along the line scan still above the glass slide and at x = 280 μm well above the $MnCO_3$ spot are presented in Figure 13(a) and Figure 13(b), respectively. Figure 13(c) shows the concentration profile of Mn^{2+} obtained scanning across the boundary between the glass substrate and the rhodochrosite feature compensated by the topography of the microstructured precipitated obtained during the preceding feedback scan. The on-set of Mn^{2+} detection in Figure 13(c) matches very well with the topographical characteristics obtained during the line scans shown in Figure 13(a).

The increase in current recorded at the UME (Figure 14(a)) during the linescan across the $MnCO_3$ feature shown in Figure 14(b) correlates with the production of Mn^{2+} above the mineral surface.

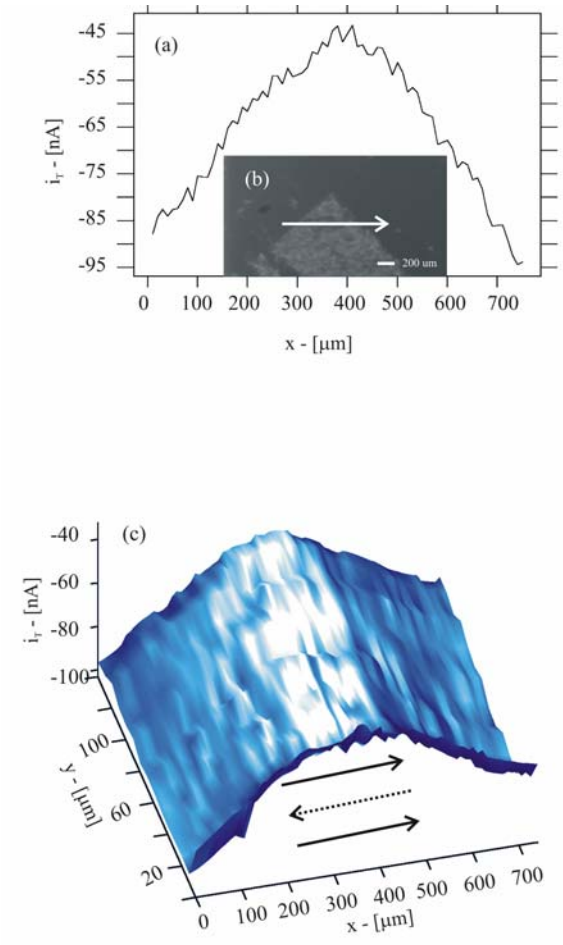

Figure 14: SECM linescan and image of the dissolution of a $MnCO_3$ spot. (a) SECM linescan across $MnCO_3$ extracted from the electrochemical image shown in (c). (b) Optical microscopy image of the investigated microstructured rhodochrosite feature. (c) SECM image of $MnCO_3$ spot obtained with a scan rate of 5 µm s^{-1}. The solid arrows indicate the scan direction.

The measurement clearly indicates that the background current is low above the glass slide. The linescan is extracted from the SECM image of the dissolution process recorded across the rhodochrosite feature shown in Figure 14(c). The solid arrow in Figure 14(c) indicates the scan direction during imaging. The dashed arrows represent the path of the electrode returning to the starting point for another linescan. SECM imaging shows that Mn^{2+} is produced above the entire area of the $MnCO_3$ spot imaged in this

measurement. The diffusion is limited to a few hundred microns in the lateral direction at these dissolution conditions. Profilometer measurements of the rhodochrosite precipitate revealed a uniform layer thickness of 1.2 μm. This value matches very well with the $MnCO_3$ spot height recorded previously during feedback measurements.

4.1.4 Conclusions

Au/Hg amalgam microelectrodes suitable for SECM measurements have been fabricated and optimized. Successful qualitative and quantitative detection of Mn^{2+} in generation/collection mode during SECM linescans and imaging using Au/Hg UMEs has been demonstrated. For the quantitative determination of the analyte concentration, the distance *d* between microelectrode and sample surface has been optimized as the current in generation/collection mode is a function of both the substrate-electrode distance and the dissolution rate of the analyte. Approach curves were successfully used with dissolved oxygen as redox mediator to determine the distance between the UME and sample surface. This strategy, however, requires precise knowledge of the electrode geometry. Therefore, the effective radius along with the dimensions and geometry of the mercury layer plated onto the gold substrate were determined for each electrode. We demonstrated that the geometry of these Au/Hg UMEs can be reproducibly fabricated, and that their electrochemical response remains consistent due to the conditioning step. We conclude that biologically relevant redox active species can be detected with high lateral resolution by combining SECM with square wave voltammetry at gold/mercury microelectrodes. This measurement concept will be extended to Fe^{2+}, H_2S, FeS, O_2, and other biogeochemically relevant trace metals in the near future.

This work was published in *The Analyst*, D. Rudolph, S. Neuhuber, C. Kranz, M. Taillefert, and B. Mizaikoff, Scanning electrochemical microscopy imaging of rhodochrosite dissolution using gold amalgam microelectrodes, 129, 443-448, 2004.

4.2 Analysis of Corrosion Processes at the Surface of Diamond-Like Carbon (DLC) Protected Zinc Selenide Waveguides

4.2.1 Amalgam Microelectrode Calibration

Au/Hg amalgam microelectrodes were calibrated by a standard addition method using 25 µL aliquots of 20 mM $ZnCl_2$ in 20 mL deaerated 1 mM acetate buffer (pH 3 adjusted with $HClO_4$) using square wave anodic stripping voltammetry (–1.6 V to –.2 V; scan rate: 5 mV/s; frequency: 40 Hz; amplitude: 25 mV) before and after SECM experiments (Figure 15(a) and (b)). The plating time for Zn^{2+} at the amalgam microelectrode was 10 seconds at -1.4 V. The stripping step of Zn^{2+} revealed a linear relationship (R = 0.996) between the Zn^{2+} concentration and the obtained current (concentration vs. current plots) within a concentration range of 100 to 500 µM. Three square wave measurements averaged per calibration point. At lower concentration levels, the relative standard deviations are < 5 %, while at higher concentrations values (1000 µM) up to 12 % are evident. It is hypothesized that these relatively high standard deviations result from incomplete stripping of Zn^{2+} prior to the next measurement. While these findings render the method semi-quantitative at the current stage of development, the main objective of this study being Zn detection due to potential imperfections of the DLC coating causing ZnSe corrosion can be clearly demonstrated. A limit of detection (LOD) for Zn of 84.78 µM +/– 1.02 was determined from the initial slope of the calibration curve and the standard deviation of blank measurements in deionized water. The expected Zn^{2+} concentration range for ZnSe corrosion is in the lower µM regime.

(a)

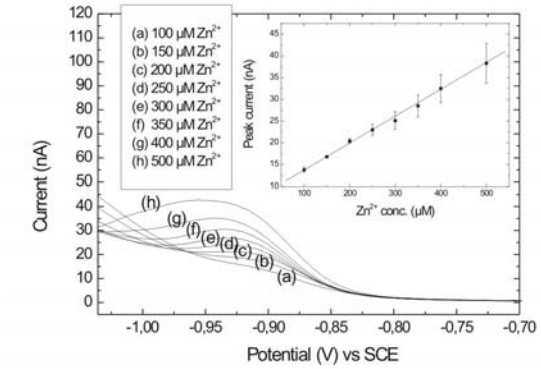

(b)

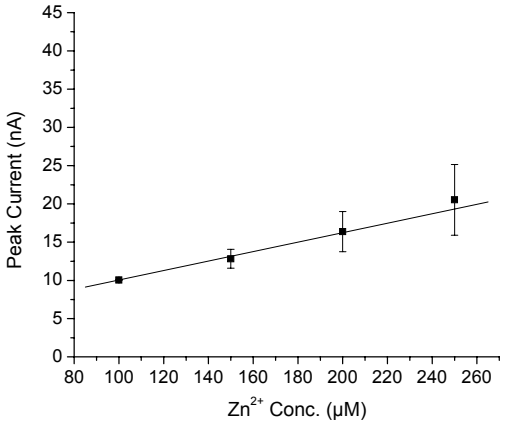

(c)

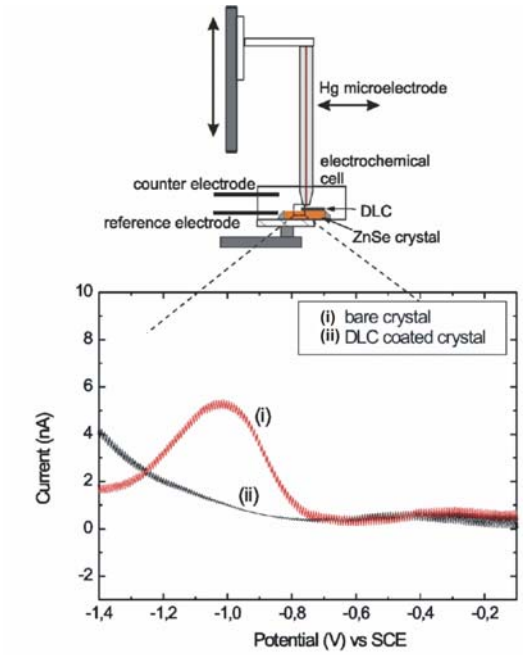

Figure 15: (a) SWASV data (scan rate: 5 mV/s; frequency: 40 Hz; amplitude: 25mV; deposition: 10 s at -1.4 V) for successive addition of Zn^{2+} to 1 mM acetate buffer. LOD: 84.78 µM +/- 1.02 before measurements. (b) Calibration curve after measurements. (c) SECM setup and recorded SWASV signals after positioning a gold/mercury amalgam UME (diam. 25 µm) above (i) an uncoated ZnSe crystal and (ii) a DLC protected ZnSe crystal immersed into a 10 mM aqueous hydrogen peroxide solution containing 1 mM acetate buffer (pH 3 adjusted with $HClO_4$).

4.2.1.1 ZnSe Corrosion Studies

Amalgam microelectrodes as surface probes in SECM measurements enable the detection of micron-sized imperfections ('pinhole detection') in the DLC coating. The corrosion of the ZnSe crystals is analyzed and quantified by profiling the Zn concentration above a DLC coated ZnSe crystal with partially removed or corrupted coating.

Square wave voltammograms were recorded with the amalgam microelectrode positioned in close proximity to either an unprotected or a DLC coated ZnSe substrate to verify the formation of Zn^{2+} during the oxidation process. Aliquots of 10 mM hydrogen peroxide containing 1 mM acetate buffer were added to the exposed uncoated or DLC protected sample prior to recording SWASV signals in order to initiate the corrosion process. An amalgam microelectrode (radius: 12.5 μm; h = 0.6820) was positioned in approx. 40 μm distance above the crystal surface using a stepper motor. A schematic of the experimental setup is shown in Figure 15(c) along with SWASVs obtained above the pristine ZnSe crystal (Figure 15(c,i)) and above a DLC protected waveguide surface (Figure 15(c,ii), respectively. Figure 15(c,i) confirms that Zn^{2+} ions are only released at the surface of the uncoated crystal due to the reaction with hydrogen peroxide. Figure 15(c,ii) indicates that no Zn^{2+} could be detected when the electrode was positioned in close proximity to the DLC coated crystal.

4.2.2 SECM Approach Curves

SECM approach curves were recorded in air-saturated 0.5 M KCl using oxygen as redox active species above an uncoated spot (330 x 600 μm) of the otherwise DLC coated

ZnSe substrate (Figure 16). The amalgam microelectrode was positioned at a height of 26 μm above the surface by fitting theoretical approach curves of an Au/Hg UME to the experimental obtained approach data (Mirkin et al., 1992).

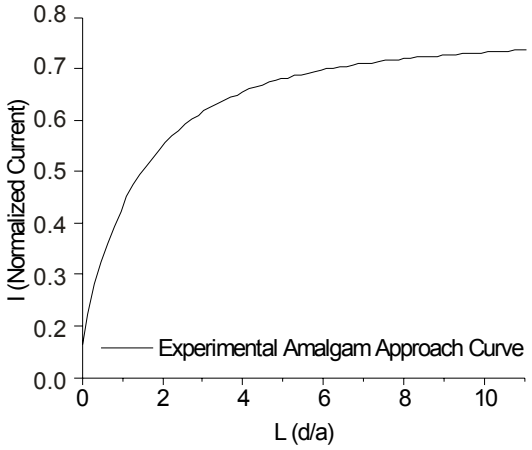

Figure 16: Negative feedback approach curve of Au/Hg electrode in 0.5 M KCl using oxygen as redox mediator.

4.2.3 SECM Imaging of DLC Waveguides

Once the tip was positioned above the substrate, the solution was replaced with 10 mM hydrogen peroxide solution containing 1 mM acetate buffer (pH 3 adjusted with $HClO_4$) initiating the corrosion process at the ZnSe substrate surface. After a waiting for a period of 45 min, square wave voltammograms (scan rate: 5 mV/s; frequency: 40 Hz; amplitude: 25 mV; deposition: 10 s at -1.4 V) were recorded at defined z-positions while moving the Au/Hg amalgam UME in increments of 25 μm along the z-axis away from the uncoated ZnSe spot (Figure 17). Hence, the Zn^{2+} concentration profile towards the bulk solution was electrochemically monitored during SECM experiments. The Zn^{2+} concentration profile is estimated using the calibration curve recorded at the amalgam

microelectrode prior to the SECM approach experiments. The inset in Figure 17 shows the correlation between the distance of the UME along the z-axis and the Zn^{2+} concentration. Within 100 µm distance from the substrate surface, the Zn^{2+} concentration decreases from 256 µM to 106 µM, which is expected in SECM generation / collection mode characterized by an inversely proportional behavior between the current measured at the UME and the distance from the source (Selzer & Mandler, 2000). During progression of the experiment Zn^{2+} ions will diffuse further into the bulk solution, which results in the detection of a notable Zn^{2+} concentrations even if the UME is positioned at a considerably larger distance away from the substrate surface.

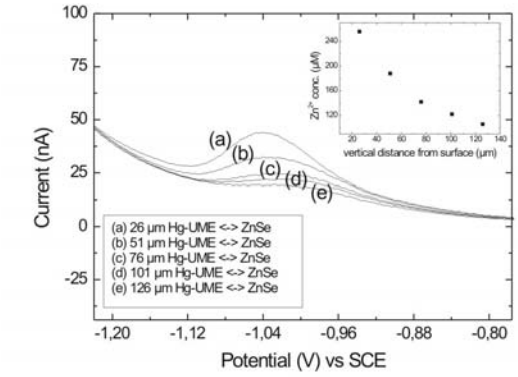

Figure 17: Square wave voltammograms recorded in 10 mM aqueous hydrogen peroxide solution containing 1 mM acetate buffer (pH 3 adjusted with $HClO_4$). Scan rate: 5 mV/s; frequency: 40 Hz; amplitude: 25 mV; deposition: 10 s at -1.4 V. The Au/Hg UME is retracted along the z-axis away from an uncoated section at the ZnSe surface in increments of 25 µm. The inset shows a plot of the Zn^{2+} concentration vs. distance of the UME in z-direction from the substrate surface.

In addition to monitoring the Zn^{2+} concentration profile in z-direction, a line scan in x-direction across a micro-scratch (approx. 70 µm in width) was recorded. The micro-scratch simulating an imperfection of the DLC layer has been produced with a pulled glass capillary using the SECM set-up. The SECM image of the scratch (Figure 18(a)) was recorded in feedback mode using oxygen as redox mediator in air-saturated 0.5 M KCl solution. The dimension of the scratch located between x = 130 µm and x = 200 µm is imaged as a change of the negative feedback current and also displayed as a linescan (Figure 18(b,i). The electrochemically derived dimensions match well with data derived from optical microscopy images recorded prior to the electrochemical experiments. As expected, the negative feedback current is decreasing when scanning over the scratched area due to increased hemispherical diffusion to the microelectrode.

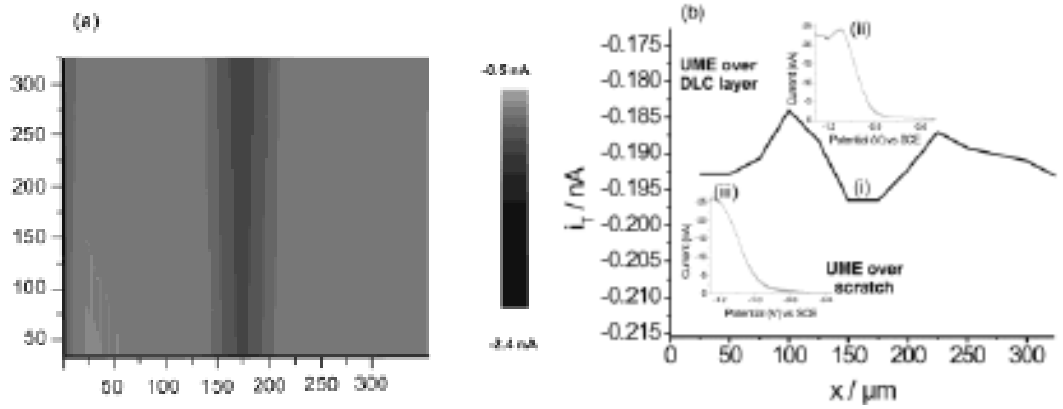

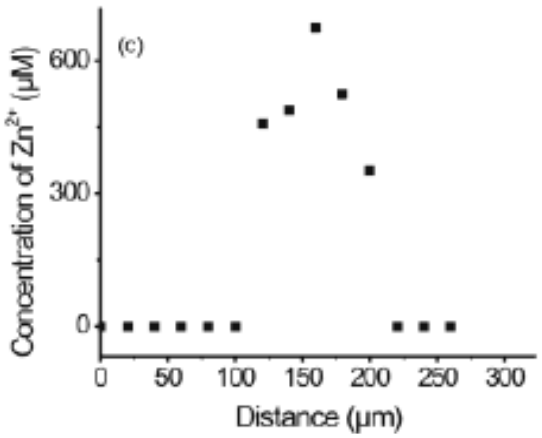

Figure 18: (a) SECM feedback mode image of a micro-scratch artificially created in the DLC coating. The image was recorded at an Au/Hg amalgam microelectrode with oxygen as redox active species in air-saturated KCl solution. i_T = -0.5 V vs. Ag/AgCl; scan speed: 2 μm s^{-1}. (b, i) Change in the amperometric current at the applied voltage of -0.5 V vs. Ag/AgCl recorded at the amalgam UME in air-saturated solution. The UME is scanned along the x-axis from the DLC coating across the micro-scratch at a scan rate of 2 μm s^{-1}. (b, ii) Typical square wave voltammogram at a position of x = 160 μm along the scan axis recorded above the micro-scratch (scan rate: 5 mV s^{-1}; frequency: 40 Hz; amplitude: 25 mV; deposition: 10 s at -1.4 V). (b, iii) Typical square wave voltammogram at x = 30 μm along the scan axis recorded above the DLC coating. Both voltammograms were recorded during the same linescan in 10 mM aqueous hydrogen peroxide solution containing 1 mM acetate buffer (pH 3 adjusted with $HClO_4$; scan rate: 5 mV s^{-1}; frequency: 40 Hz; amplitude: 25 mV; deposition: 10 s at -1.4 V). (c) Topography-corrected concentration profile of Zn^{2+} across the micro-scratch.

The solution was then replaced with 10 mM aqueous hydrogen peroxide solution containing 1 mM acetate buffer (pH 3 adjusted with $HClO_4$) initiating the dissolution of ZnSe at the artificially created defect of the DLC coating within a period of 85 min. The Au/Hg amalgam UME was scanned at a constant height across the exposed section (micro-scratch) of the ZnSe crystal and the differential current of square wave voltammetry was recorded during the SECM line scan in generation collection mode at intervals of 20 μm. Two representative voltammograms are shown (Figure 18(b,ii) & (b,iii)). Figure 18(c) shows the concentration profile of Zn^{2+} corrected by the topography in x-direction across the micro-scratch. It is evident that the oxidative process dissolves

the ZnSe crystal at the exposed area and releases Zn^{2+} ions, as shown in the related voltammograms (Figure 18(b,ii)). The characteristic Zn^{2+} peak is located at approx. -1.0 V, while the voltammogram recorded above the DLC protected area next to the micro-scratch (Figure 18(b,iii)) yields no signal at this potential. The topography-corrected concentration profile shown in Figure 18(c) was calculated from the calibration curves recorded at the amalgam microelectrode prior to the SECM experiments and the SECM feedback data, respectively. Hence, we have demonstrated the ability of utilizing square wave voltammetry for laterally resolved detection of Zn^{2+} ion release across the micro-scratch section of the DLC layer.

4.2.4 Conclusions

This study investigated the corrosion barrier properties of IR-transparent diamond-like carbon (DLC) thin films coated onto ZnSe waveguides in corrosive aqueous environments with scanning electrochemical microscopy (SECM). The applied technique proves the efficiency of DLC coatings with a thickness of approx. 100 nm as protective layers at ZnSe IR waveguide surfaces. The innovative application of Au/Hg amalgam microelectrodes based square wave voltammetric SECM experiments provided laterally resolved electrochemical information on the release of Zn^{2+} ions during the corrosion process. The lateral resolution is limited to the micro-range due to the diameter (25 μm) of the applied amalgam microelectrodes.

This work was published in *Langmuir*, M. Janotta, D. Rudolph, A. Kueng, C. Kranz, H.-S. Voraberger, W. Waldhauser, and B. Mizaikoff, Analysis of corrosion processes at the surface of diamond-like carbon protected zinc selenide waveguides, 20, 8634-8640, 2004.

4.3 Detection of Metal-Reducing Enzyme Complexes by Scanning Electrochemical Microscopy (SECM)

4.3.1 Amalgam Microelectrode Calibration

The current response of the fabricated Pt/Hg amalgam electrodes varies with the effective radius of the microelectrode and the volume of mercury plated onto the electrode surface. Individual amalgam microelectrodes were calibrated before and after SECM experiments using anodic and cathodic square wave voltammetry in bulk solution (-1.6 V to -0.1 V; scan rate: 50 mVs^{-1}; frequency: 40 Hz; amplitude: 15mV) by standard addition (Figure 19).

(a) (b)

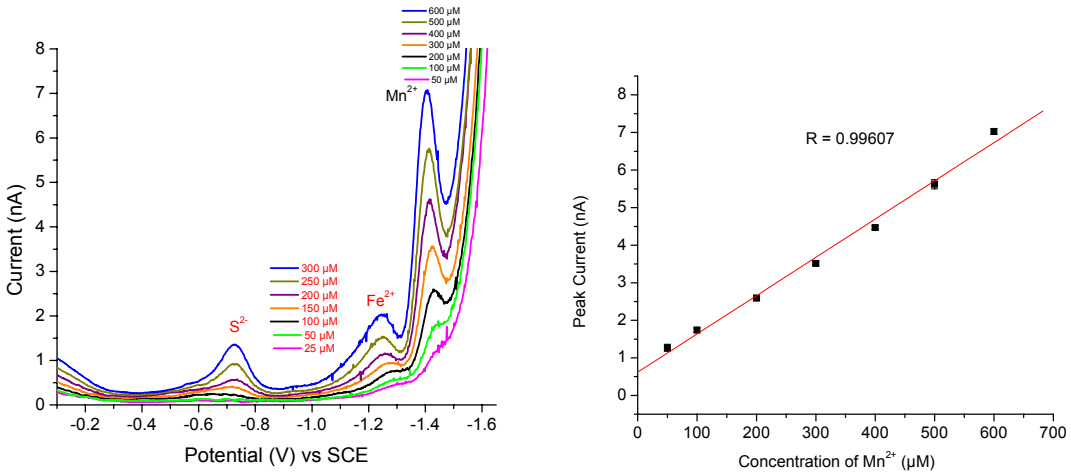

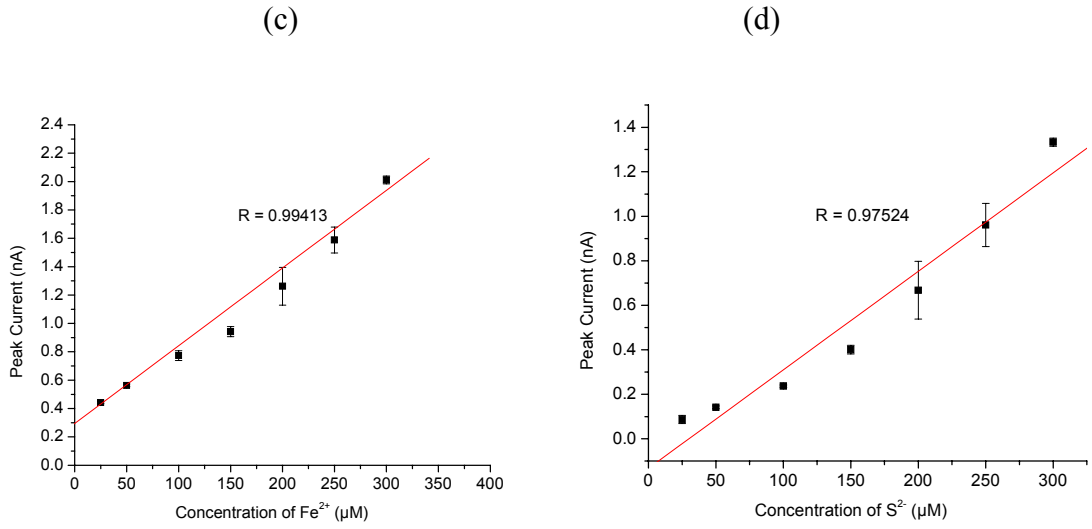

Figure 19: (a) Square-wave voltammograms obtained at a 25 µm Pt/Hg amalgam microelectrode calibrated (in bulk solution) for Mn^{2+}, Fe^{2+}, and S^{2-} in 10 mL degassed tris-acetate buffer (pH 7.5) with standard addition of 25 µL of 40 mM $MnCl_2$, 20mM $FeCl_2$, and 20mM Na_2S stock solutions. (b) Mn^{2+}, (c) Fe^{2+}, and (d) S^{2-} calibration curves recorded at Pt/Hg amalgam microelectrode. Note that some error bars at lower concentrations are smaller than the symbol size.

The calibration curves were obtained in 10 mL degassed tris-acetate buffer with standard addition of 25 µL of 40 mM $MnCl_2$, 20mM $FeCl_2$, and 20mM Na_2S stock solutions. The stripping step revealed a linear relationship between concentration and the obtained current (concentration vs. current plots) of Mn^{2+}, Fe^{2+}, and S^{2-} within a concentration range of 25 – 350 µM. A limit of detection (LOD) for Mn^{2+} (87 µM +/- 4), Fe^{2+} (13 µM +/- 9), and S^{2-} (25 µM +/- 5) was determined from the initial slope of the calibration curve and the standard deviation of blank measurements in tris-acetate buffer.

4.3.2 SECM Approach Curves

In order to position the Pt/Hg amalgam microelectrode in close proximity to the gel surface, z-approach curves were recorded using the reduction of oxygen in 0.1 M tris-

acetate buffer solution (pH 7.5) (Figure 20). The Pt/Hg amalgam microelectrode was positioned in an area containing no redox protein bands. Once the positioning of the microelectrode was completed, the solution and the environmental chamber were purged with argon.

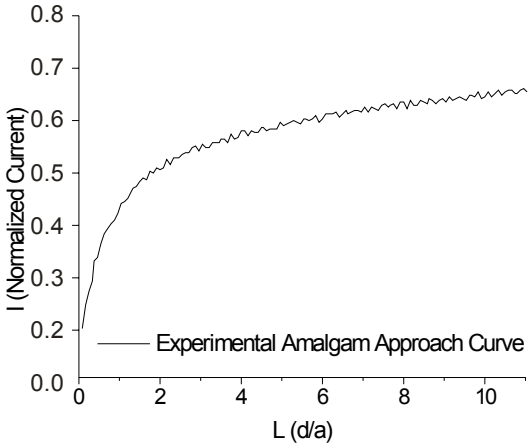

Figure 20: Negative feedback approach curve of Pt/Hg microelectrode in 0.1 M tris-acetate buffer solution (pH 7.5) using oxygen as redox mediator.

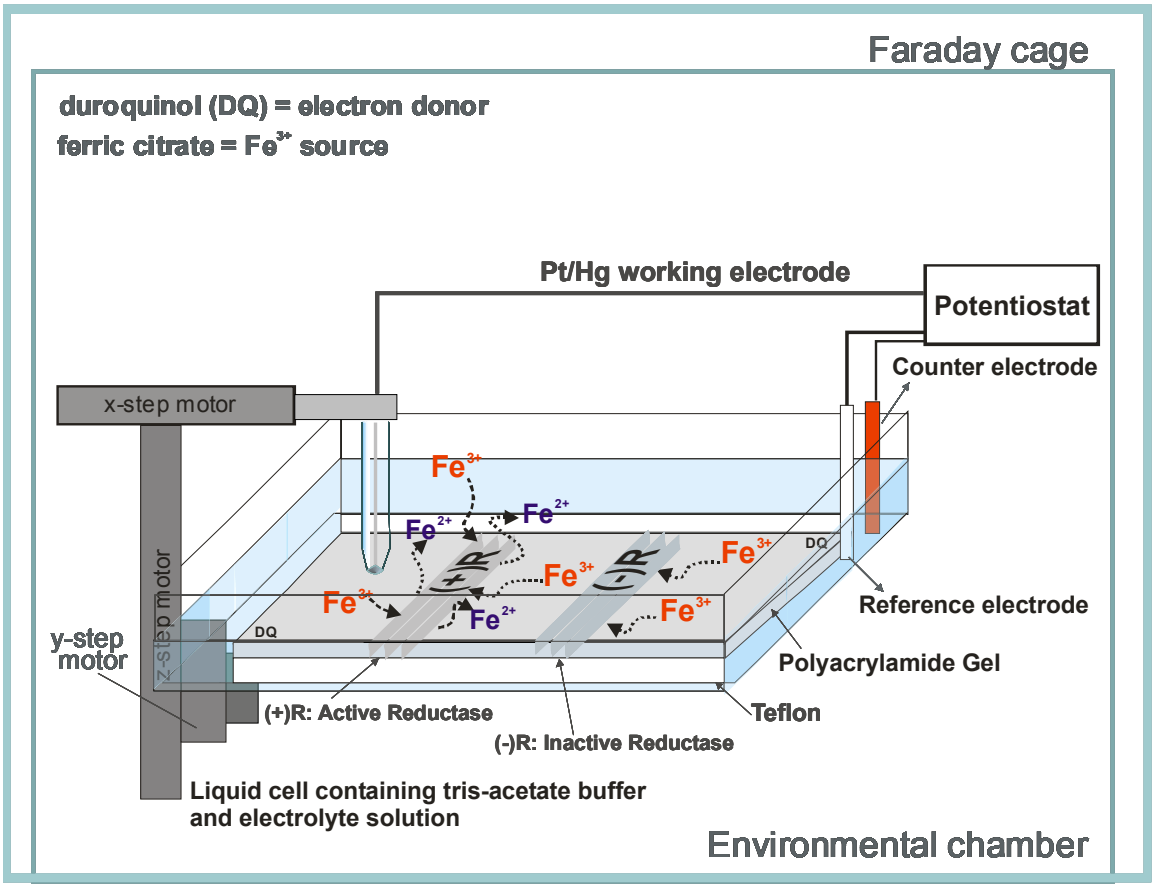

Figure 21: Scheme of the SECM experiment conducted in generation/collection mode at Pt/Hg amalgam microelectrodes for the detection of Fe^{3+} reduction catalyzed by a reductase / reductase complex contained in a polyacrylamide gel after electrophoretic separation.

4.3.3 SECM Gel Reader

The source for Fe^{3+} ions was a degassed 10 mM ferric citrate solutions in 0.1 M tris-acetate buffer. Degassed 10 mM ferrozine solution in 0.1 M tris-acetate buffer, which is usually applied as a staining agent for colorimetric Fe^{2+} tests, was used as a complexant for Fe^{2+}. These solutions were inserted inside the environmental chamber via syringe and tubing attached to the Teflon cell. The oxygen content within the environmental chamber was continuously monitored with a commercial oxygen probe (ThermoOrion 810A+, Beverly, MA) ensuring that the oxygen content was below 2.5

ppm in the chamber. After adding the electron acceptor to the solution, the Pt/Hg amalgam microelectrode was scanned across the native gel at a fixed height of 36 μm determined by the recorded approach curve. The scan was stopped above an active protein band, which was verified in comparison with a gel that had been stained for Fe (III) activity.

After positioning above an active zone, a series of voltammograms over a period of 1 hour were recorded (Figure 22). The square wave voltammograms recorded at the beginning of the experiment predominantly show a Fe^{3+} peak at -0.4 V vs. Ag/AgCl, as expected (Figure 22(a)). This peak results from the addition of ferric citrate. The sodium ions present in the buffer solution cause a steep increase at -1.5 V vs. Ag/AgCl. Sodium ions were not excluded from the buffered solution since sodium is always present also in the natural environment of the bacteria. The shoulder peak at -1.4 V vs. Ag/AgCl reveals the evolution of Fe^{2+} over time resulting from an active reductase protein band catalyzing the reduction of Fe^{3+} (Figure 22(a)). The square wave voltammograms in Figure 22 were recorded over a period of 12 minutes. After 7 minutes, the Fe^{3+} concentration has already significantly decreased, and an additional peak in the voltammogram indicating the formation of an iron-sulfur complex is evolving at -0.6 V vs. Ag/AgCl (Figure 22(b)). In order to determine the origin of the sulfur species, control experiments above a native gel, which contains no proteins (blank gel) were performed.

(a) 0 min. (b) 7 min.

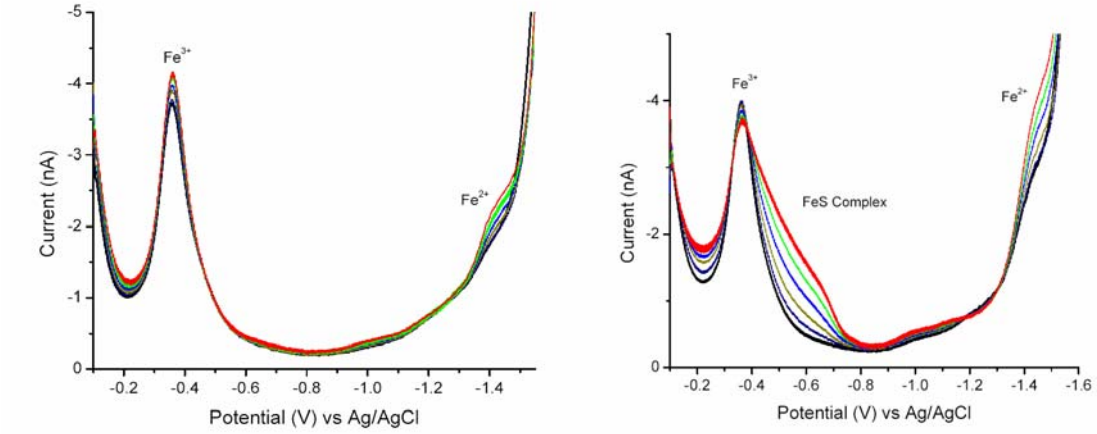

(c) 10 min. (d) 12 min.

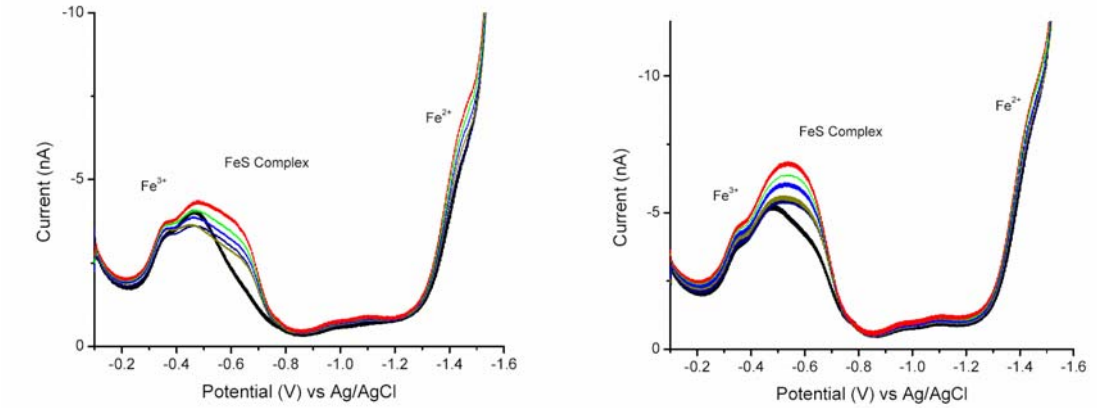

Figure 22: Square wave voltammograms recorded at a 25 µm Pt/Hg amalgam UME positioned in close proximity above the native gel recorded over a period of 20 min. (a-d). The active band contains redox proteins. The experiments were performed in 1 mL of 0.1 M tris-acetate buffer containing 10 mM ferrozine and 10 mM ferric citrate under inert argon atmosphere with a remaining oxygen concentration of 2.5 ppm. (a) Start of measurements at 0 min after positioning above the band, (b) after 7 min, (c) after 10 min, and (d) after 12 min. All potentials are recorded vs. Ag/AgCl.

As clearly evident from the control square wave voltammograms (see Figure 23 & Table 3), the gel matrix contains a small amount of sulfur, which is detected at the Pt/Hg amalgam microelectrode at -0.6 V vs. Ag/AgCl. The detected sulfur concentration above the control gel, however, remains at a constant level / concentration (Figure 23) of 44.07

μM +/- 9.54. The square wave voltammograms shown in Figure 23 are an overlay of 5 voltammograms recorded over a period of 1 hour (in intervals of 10 min) in which the height of the sulfur peak does not significantly change / increase. There is no other source of sulfur in these experiments, as all solutions were tested in bulk experiments for sulfur peaks. The peak of the sulfur species recorded above active reductase proteins keeps increasing with time (Figure 22), and therefore indicates that the sulfur species originates from the Fe^{3+}-reducing protein complex.

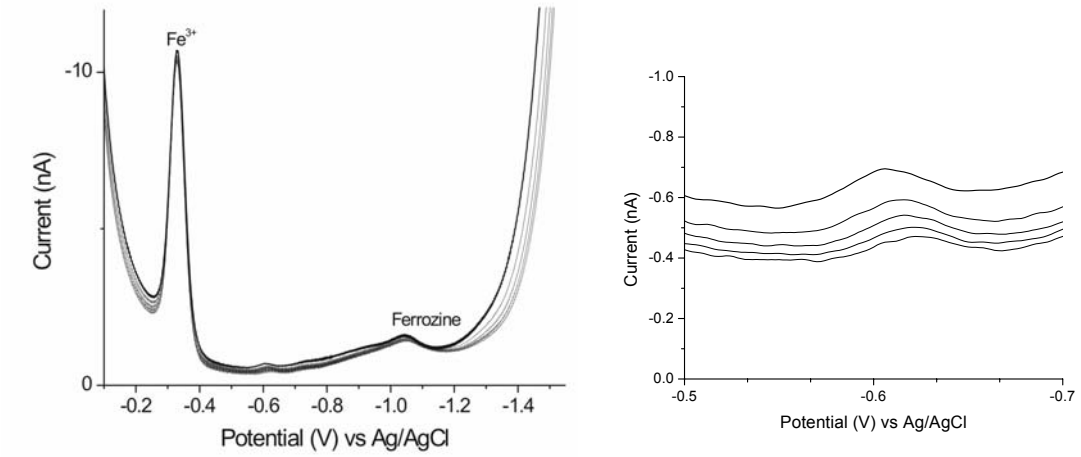

Figure 23: (Left) Overlay of 5 square wave voltammograms recorded over a period of 1 hour (in 10 min intervals) (Right) Zoom in view of sulfur peak region. Measurements performed under the same experimental conditions described for the results shown above (Figure 22)

Table 3: The same experiments as described in Figure 22 were repeatedly performed above a control gel which contains either no separated compound (blank), an active reductase (R(+)), or an inactive reductase (R(-)) at the same experimental conditions.

Sulfur Species	(+) Ferric Citrate			(-) Ferric Citrate			DQ
	(+) R	(-) R	Blank	(+) R	(-) R	Blank	
$S_2O_3^{2-}$	(+)	(+)	(+)	(+)	(+)	(+)	(-) (+)
SO_4^{2-}	(+)	(+)	(+)	(+)	(+)	(+)	(-) (+)
SO_3^{2-}	(+)	(+)	(+)	(+)	(+)	(+)	(-) (+)
(-)	(+)	(+)	(+)	(+)	(+)	(+)	(-) (+)

(+) means added and (-) means removed from system

Control experiments, as described above, were repeatedly performed above a native gel without redox proteins bands (blank), an active reductase protein band (R(+)), and an inactive reductase (R(-)) maintaining identical experimental conditions. The following voltammetric parameters were used for the stripping process: -1.6 V to -0.1 V; scan rate: 50 mVs^{-1}; frequency: 40 Hz; amplitude: 15mV. At these conditions, the anodic and cathodic stripping peak was not significantly affected by the presence of durquinol (DQ) or ferrozine.

Additional strains of the microbe were separated and investigated in the SECM In an effort to identify the involved sulfur species. A SECM line scan in x direction across the active and inactive zones of a fresh native gel (approx. 1000 µm between zones) was recorded. The amalgam microelectode was scanned at a constant height across the

reductase zones of the gel and the differential current of the anodic and cathodic square wave stripping voltammetry was recorded during the SECM line scan at intervals of 125 μm. Two representative voltammograms are shown in Figure 24(a) and (b). The square wave voltammograms recorded over the active zone of the gel show a Fe^{3+} peak at -0.4 V and a Fe^{2+} peak at -1.43 V (vs. Ag/AgCl) (Figure 24(a)), due to the enzymatic reduction of Fe^{3+} (from the added ferric citrate). The shoulder (anodic scan) and peak (cathodic scan) found at -0.5 V vs. Ag/AgCl reveals the evolution of S^{2-} and FeS resulting from the active reductase protein band (Figure 24(a)). The square wave voltammograms recorded above the inactive reductase zone of the gel show the expected Fe^{3+} peak at -0.4 V vs. Ag/AgCl (Figure 24(b)) due to the added ferric citrate. However, no Fe^{2+} or FeS peaks were observed in the inactive zone. There is a low level / concentration of sulfur (S^{2-}) detected in this zone that remains constant. Figure 24(c) shows the concentration profile of Fe^{3+}, FeS, and Fe^{2+} in x-direction across the gel zones. It is evident that the enzymatic process reduces the Fe^{3+} at the active zone and releases Fe^{2+} ions. A sulfur species (likely a combination of S^{2-} and FeS) is also released by the reductase in the active zone. The concentration profile shown in Figure 24(c) was calculated from the calibration curves recorded at the amalgam microelectrode prior to the SECM experiments. There was a moderate amount of literature that aided in FeS and sulfide peak identification (Figure 25) (Davison, Buffle, & Devitre, 1988; Rozan, Theberge & Luther, 1997; Theberge, & Luther, 2000; Billon, Ouddane, & Boughriet, 2001).

(a)

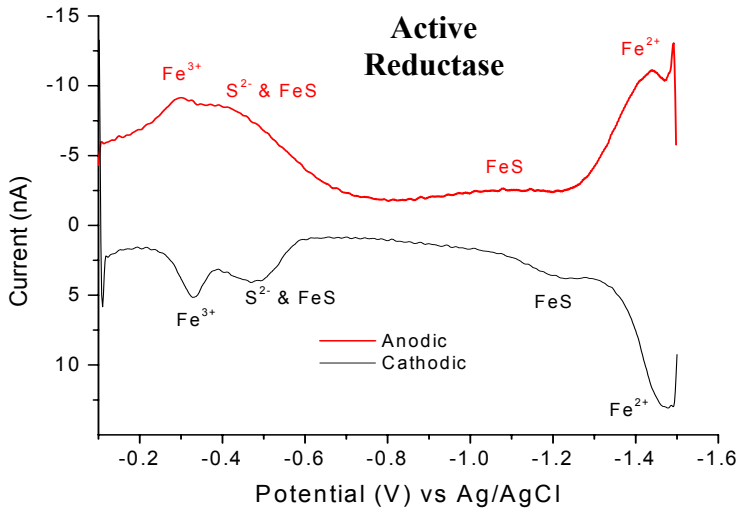

(b)

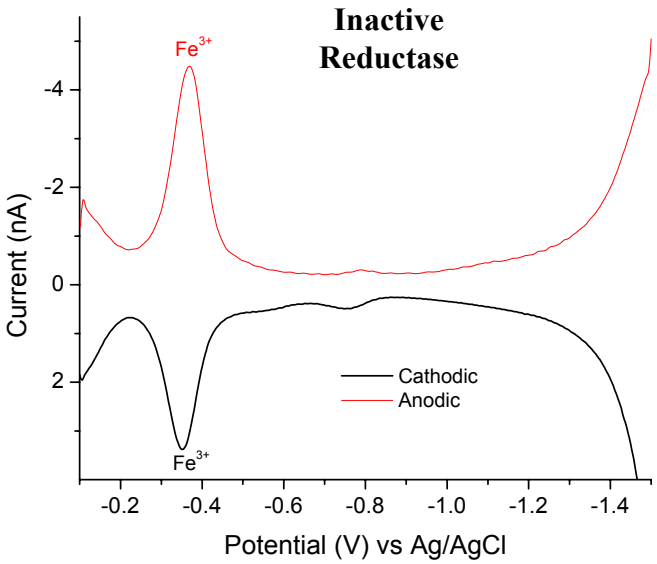

Figure 24: Square wave voltammograms recorded at a 25 µm Pt/Hg amalgam UME positioned in close proximity above the native gel. (a) The band contains active redox proteins. (b) The band contains inactive redox proteins. Top: Anodic scan. Bottom: Cathodic scan. (c) Concentration profile of Fe^{3+}, FeS, and Fe^{2+} across the active and inactive zones of the gel. The experiments were performed in 1 mL of 0.1 M tris-acetate buffer containing 10 mM ferric citrate under inert argon atmosphere containing 2.5 ppm oxygen. All potentials are recorded vs. Ag/AgCl.

Figure 24 Continued
(c)

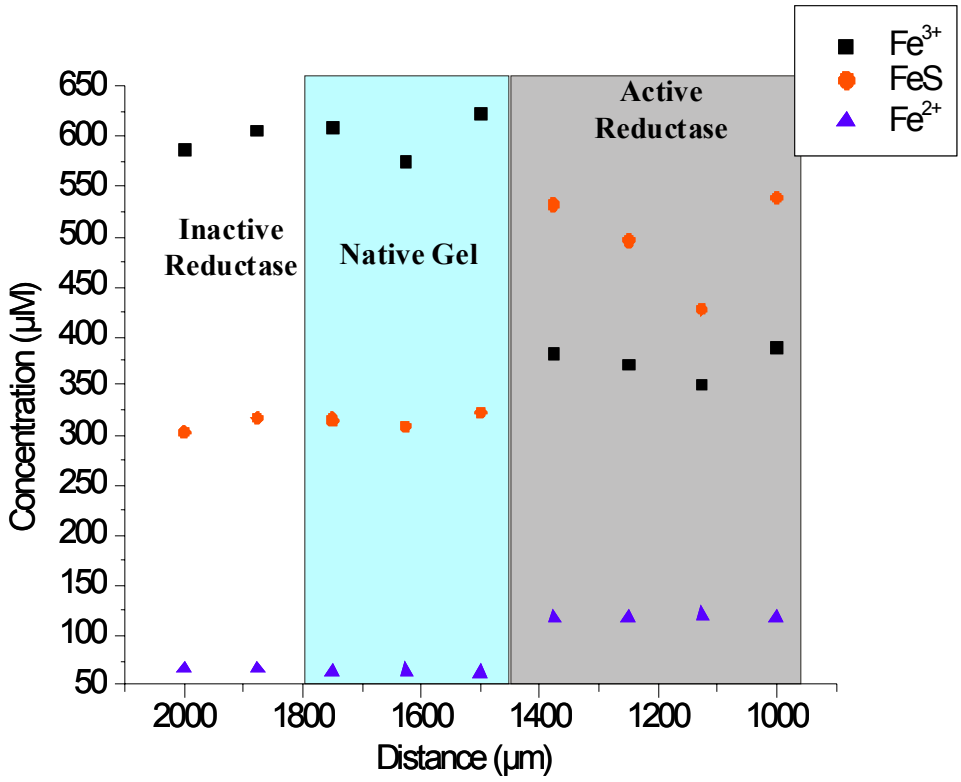

Figure 24: Square wave voltammograms recorded at a 25 µm Pt/Hg amalgam UME positioned in close proximity above the native gel. (a) The band contains active redox proteins. (b) The band contains inactive redox proteins. Top: Anodic scan. Bottom: Cathodic scan. (c) Concentration profile of Fe^{3+}, FeS, and Fe^{2+} across the active and inactive zones of the gel. The experiments were performed in 1 mL of 0.1 M tris-acetate buffer containing 10 mM ferric citrate under inert argon atmosphere containing 2.5 ppm oxygen. All potentials are recorded vs. Ag/AgCl.

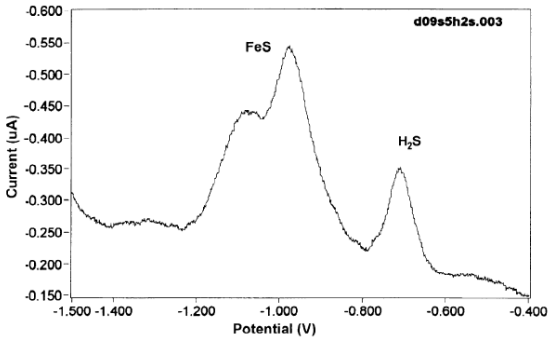

Figure 25: Representative SWV voltammogram of hydrothermal vent fluid. Reproduced from Theberge & Luther 1997.

4.3.4 Conclusions

Square wave voltammograms were recorded with the amalgam microelectrode positioned in close proximity to an active protein band separated in the gel in order to verify the formation of Fe^{2+} during the enzymatic reduction process. Fe (III) was added in the form of iron citrate in order to provide the separated proteins an iron source. The activity of the protein complex is reflected in a decrease of Fe (III) and an increase in Fe (II) with time. Our measurements also indicate that a sulfur compound must be provided by the isolated reductase proteins. To prove the fact that only Fe^{3+} reducing active protein bands show an additional sulfur species, positive and negative control experiments on pristine gels and with protein containing gels were performed. The control data shows evidence that the observed peaks at -0.6 V and -1.4 V vs. Ag/AgCl only occur in presence of active proteins / protein complexes in the gel matrix.

It is hypothesized that the microbe has evolved a dissimilatory Fe (III) reduction pathway, which is based on assimilatory sulfate reduction. These initial experiments indicate that sulfur is a central intermediate in the respiratory Fe (III) reductase complex of the microbe. Furthermore, it has been confirmed that Fe^{2+} and sulfur species are only

released at bands of the gel where active reductases are located. It is verified that only much lower levels of Fe^{2+} and sulfur can be found above inactive zones, which allows the conclusion that these levels are detected only due to the continuous release and diffusion of Fe^{2+} and sulfur from the active zone approximately 1000 μm away. These results provide evidence that the assimilatory sulfate reduction pathway is involved in the catalytic activity of the respiratory Fe (III) reductase complex of *shewanella oneidensis*. The experiments in this study demonstrate the ability of square wave voltammetry at amalgam microelectrodes in combination with SECM for the laterally resolved detection of protein activity across sections of native gel matrices.

Chemical species involved in or generated by respiratory reductases from metal-reducing bacteria can be simultaneously detected after separation in native gels. This novel protein activity identification strategy has the potential to revolutionize the current methodologies used for gel reading. The positioning of a Pt/Hg amalgam microelectrode in close proximity above protein bands embedded in a native gel after separation enables the read-out of active reductase proteins by detecting their redox activity. This work strives to provide insight on the mechanisms of microbial metal respiration.

The experiments described above clearly suggest that the demonstrated concept of utilizing SECM with amalgam microelectrodes as a read-out device for gels containing redox active proteins or complexes is feasible. This approach is capable of assisting and surpassing current methods in identifying a variety of active proteins related to metal-reducing bacteria respiration in marine sediments. Hence, redox proteins which cannot be stained such as e.g. sulfur reductases are now directly accessible with SECM using amalgam microelectrodes.

A manuscript of these studies is in preparation to *Nature Methods*, D. Rudolph, D. Bates, T. DiChristina, C. Kranz, and B. Mizaikoff, Detection of metal-reducing enzyme complexes in native 2D gels by scanning electrochemical microscopy (SECM), in preparation, 2005.

5 CONCLUSIONS AND OUTLOOK

Au/Hg microelectrodes suitable for SECM measurements have been fabricated and optimized. Successful qualitative and quantitative detection of Mn^{2+} in generation/collection mode during SECM linescans and imaging using Au/Hg UMEs has been demonstrated. For quantitative determination of the analyte concentration, the distance *d* between microelectrode and sample surface has to be optimized as the current in generation/collection mode is a function of both the substrate-electrode distance and the dissolution rate of the analyte. We successfully used approach curves with dissolved oxygen as redox mediator to determine the distance between the UME and sample surface. However, this strategy requires precise knowledge of the electrode geometry. The effective radius along with the dimensions and geometry of the mercury layer plated onto the gold substrate were determined for each electrode. We demonstrated that the geometry of these Au/Hg UMEs can be reproducibly fabricated and that their electrochemical response remains consistent due to the conditioning step. We conclude that biologically relevant redox active species can be detected with high lateral resolution by combining SECM with square wave voltammetry at gold/mercury microelectrodes. This measurement concept was extended to Zn^{2+}, Fe^{2+}, FeS, and other biogeochemically relevant trace metals.

Our overall objective is to reduce the spatial resolution of SECM to a few tens of nanometers using much smaller electrodes. First results indicate that this concept can be extended to mercury microelectrodes integrated into AFM cantilevers by electrodeposition of mercury onto integrated gold micro- and nanoelectrodes. Plating and polarization times of amalgam nanoelectrodes have been optimized in order to produce

stable thin-film mercury electrodes. These AFM-tip integrated amalgam nanoelectrodes will provide yet unachieved lateral resolution for detection of redox active species at substrate-liquid interfaces. The inherent separation of the substrate topography from the analyte detection during a simultaneous measurement will furthermore pioneer nanoscale exploration of manganese and iron reductions occurring at biogeochemically relevant microbe/mineral interfaces.

REFERENCES

Amphlett, J. L., & Denuault, G. (1998). Scanning Electrochemical Microscopy (SECM): An Investigation of the Effects of Tip Geometry on Amperometric Tip Response. *Journal of Physical Chemistry B, 102*(49), 9946-9951.

Arnold, R. G., DiChristina, T. J., & Hoffmann, M. R. (1988). Reductive dissolution of iron(III) oxides by Pseudomonas sp. 200. *Biotechnology and Bioengineering, 32*(9), 1081-1096.

Barbeira, P. J. S., & Stradiotto, N. R. (1997). Simultaneous determination of trace amounts of zinc, lead and copper in rum by anodic stripping voltammetry. *Talanta, 44*(2), 185-188.

Bard, A. J., Fan, F. R. F., Kwak, J., & Lev, O. (1989). Scanning electrochemical microscopy. Introduction and principles. *Analytical Chemistry, 61*(2), 132-138.

Bard, A. J., Fan, F. R. F., & Mirkin, M. V. (1994). Scanning electrochemical microscopy. *Electroanalytical Chemistry, 18*, 243-373.

Basame, S. B., & White, H. S. (1995). Scanning electrochemical microscopy of native titanium oxide films. Mapping the potential dependence of spatially-localized electrochemical reactions. *Journal of Physical Chemistry, 99*(44), 16430-16435.

Berner, R. A., & Petsch, S. T. (1998). Perspectives: Paleoclimate. The sulfur cycle and atmospheric oxygen. *Science (Washington, D. C.), 282*(5393), 1426-1427.

Billon, G., Ouddane, B., & Boughriet, A. (2001). Chemical speciation of sulfur compounds in surface sediments from three bays (Fresnaye, Seine and Authie) in northern France, and identification of some factors controlling their generation. *Talanta, 53*(5), 971-981.

Brendel, P. J., & Luther, G. W., III. (1995). Development of a Gold Amalgam Voltammetric Microelectrode for the Determination of Dissolved Fe, Mn, O2, and S(-II) in Porewaters of Marine and Freshwater Sediments. *Environmental Science and Technology, 29*(3), 751-761.

Calvert, S. E., & Price, N. B. (1972). Diffusion and reaction profiles of dissolved manganese in the pore waters of marine sediments. *Earth and Planetary Science Letters, 16*(2), 245-249.

Ciani, I., Daniele, S., Bragato, C., & Baldo, M. A. (2003). Stability of mercury-coated platinum microelectrodes upon touching a solid surface in scanning electrochemical microscopy (SECM) experiments. *Electrochemistry Communications, 5*(4), 354-358.

Colyer, C. L., Luscombe, D., & Oldham, K. B. (1990). Growth of mercury electrodeposits on an inlaid disk. Voltammetric theory and experiments. *Journal of Electroanalytical Chemistry and Interfacial Electrochemistry, 283*(1-2), 379-387.

Daniele, S., Bragato, C., Baldo, M. A., Wang, J., & Lu, J. (2000). The use of a remote stripping sensor for the determination of copper and mercury in the Lagoon of Venice. *Analyst (Cambridge, United Kingdom), 125*(4), 731-735.

Daniele, S., Bragato, C., Ciani, I., & Baldo, M. A. (2003). Sphere-cap mercury microelectrodes for scanning electrochemical microscopy above an insulating substrate. *Electroanalysis, 15*(7), 621-628.

Davison, W., Buffle, J., & Devitre, R. (1988). Interpretation of speciation measurements: a case study. Direct polarographic determination of molecular oxygen, iron(II), manganese(II), sulfur(-II), and related species in anoxic waters. *Pure and Applied Chemistry, 60*(10), 1535-1548.

de Wit, J. H. W. (2001). New knowledge on localized corrosion obtained from local measuring techniques. *Electrochimica Acta, 46*(24-25), 3641-3650.

Desmond, D., Lane, B., Alderman, J., Hill, M., Arrigan, D. W. M., & Glennon, J. D. (1998). An environmental monitoring system for trace metals using stripping voltammetry. *Sensors and Actuators, B: Chemical, B48*(1-3), 409-414.

DiChristina, T. J., Moore, C. M., & Haller, C. A. (2002). Dissimilatory Fe(III) and Mn(IV) reduction by Shewanella putrefaciens requires ferE, a homolog of the pulE (gspE) type II protein secretion gene. *Journal of Bacteriology, 184*(1), 142-151.

Engstrom, R. C., Weber, M., Wunder, D. J., Burgess, R., & Winquist, S. (1986). Measurements within the diffusion layer using a microelectrode probe. *Analytical Chemistry, 58*(4), 844-848.

Froelich, P. N., Klinkhammer, G. P., Bender, M. L., Luedtke, N. A., Heath, G. R., Cullen, D., et al. (1979). Early oxidation of organic matter in pelagic sediments of the eastern equatorial Atlantic: suboxic diagenesis. *Geochimica et Cosmochimica Acta, 43*(7), 1075-1090.

Fulian, Q., Fisher, A. C., & Denuault, G. (1999). Applications of the Boundary Element Method in Electrochemistry: Scanning Electrochemical Microscopy, Part 2. *Journal of Physical Chemistry B, 103*(21), 4393-4398.

Ghiorse, W. C. (1988). The biology of manganese transforming microorganisms in soil. *Developments in Plant and Soil Sciences, 33*(Manganese Soils Plants), 75-85.

Horrocks, B. R., Mirkin, M. V., & Bard, A. J. (1994). Scanning Electrochemical Microscopy. 25. Application to Investigation of the Kinetics of Heterogeneous Electron Transfer at Semiconductor (WSe2 and Si) Electrodes. *Journal of Physical Chemistry, 98*(37), 9106-9114.

Janotta, M., Rudolph, D., Kueng, A., Kranz, C., Voraberger, H.-S., Waldhauser, W., et al. (2004). Analysis of Corrosion Processes at the Surface of Diamond-Like Carbon Protected Zinc Selenide Waveguides. *Langmuir*, ACS ASAP.

Johnson, K. S. (1982). Solubility of rhodochrosite (MnCO3) in water and seawater. *Geochimica et Cosmochimica Acta, 46*(10), 1805-1809.

K. Xu, S. C. D., and G.W. Luther III. (1997). *Corrosion/97, 300*.

Katemann, B. B., Inchauspe, C. G., Castro, P. A., Schulte, A., Calvo, E. J., & Schuhmann, W. (2003). Precursor sites for localized corrosion on lacquered tin plates visualized by means of alternating current scanning electrochemical microscopy. *Electrochimica Acta, 48*(9), 1115-1121.

Kleber, C., & Schreiner, M. (2003). In situ TM-AFM investigations of the influence of zinc and tin as alloy constituents of copper to the early stages of corrosion. *Applied Surface Science, 217*(1-4), 294-301.

Kwak, J., & Anson, F. C. (1992). Monitoring the ejection and incorporation of ferricyanide [Fe(CN)63-] and ferrocyanide [Fe(CN)64-] counterions at protonated poly(4-vinylpyridine) coatings on electrodes with the scanning electrochemical microscope. *Analytical Chemistry, 64*(3), 250-256.

Kwak, J., & Bard, A. J. (1989). Scanning electrochemical microscopy. Theory of the feedback mode. *Analytical Chemistry, 61*(11), 1221-1227.

Lackner, J. M., Stotter, C., Waldhauser, W., Ebner, R., Lenz, W., & Beutl, M. (2003). Pulsed laser deposition of diamond-like carbon coatings for industrial tribological applications. *Surface and Coatings Technology, 174-175*, 402-407.

Lee, Y., Amemiya, S., & Bard, A. J. (2001). Scanning Electrochemical Microscopy. 41. Theory and Characterization of Ring Electrodes. *Anal. Chem., 73*(10), 2261-2267.

Liljeroth, P., Johans, C., Slevin, C. J., Quinn, B. M., & Kontturi, K. (2002). Micro ring-disk electrode probes for scanning electrochemical microscopy. *Electrochemistry Communications, 4*(1), 67-71.

Lister, T. E., & Pinhero, P. J. (2003). The effect of localized electric fields on the detection of dissolved sulfur species from Type 304 stainless steel using scanning electrochemical microscopy. *Electrochimica Acta, 48*(17), 2371-2378.

Liu, H. Y., Fan, F. R. F., Lin, C. W., & Bard, A. J. (1986). Scanning electrochemical and tunneling ultramicroelectrode microscope for high-resolution examination of electrode surfaces in solution. *Journal of the American Chemical Society, 108*(13), 3838-3839.

Lloyd, J. R., Sole, V. A., Van Praagh, C. V. G., & Lovley, D. R. (2000). Direct and Fe(II)-mediated reduction of technetium by Fe(III)-reducing bacteria. *Applied and Environmental Microbiology, 66*(9), 3743-3749.

Lovely, D. R. (1991). Dissimilatory Fe(III) and Mn(IV) reduction. *Microbiol. Rev., 55*, 259-287.

Lovley, D. R., Coates, J. D., Saffarini, D. A., & Lonergan, D. J. (1997). Dissimilatory iron reduction. *Transition Metals in Microbial Metabolism*, 187-215.

Macpherson, J. V., Unwin, P. R., Hillier, A. C., & Bard, A. J. (1996). In-Situ Imaging of Ionic Crystal Dissolution Using an Integrated Electrochemical/AFM Probe. *Journal of the American Chemical Society, 118*(27), 6445-6452.

Marcus, P., Maurice, V., Costa, D., & Galtayries, A. (2002). The contribution of surface analysis to corrosion science: Historical background and current status. *Proceedings - Electrochemical Society, 2002-13*(Corrosion Science), 117-137.

Maurice, V., Klein, L. H., & Marcus, P. (2002). Atomic-scale investigation of the localized corrosion of passivated nickel surfaces. *Surface and Interface Analysis, 34*(1), 139-143.

Mirkin, M. V., Fan, F. R. F., & Bard, A. J. (1992). Scanning electrochemical microscopy. Part 13. Evaluation of the tip shapes of nanometer size microelectrodes. *Journal of Electroanalytical Chemistry, 328*(1-2), 47-62.

Mirkin, M. V., & Horrocks, B. R. (2000). Electroanalytical measurements using the scanning electrochemical microscope. *Anal. Chim. Acta, 406*(2), 119-146.

Myers, C. R., & Myers, J. M. (1992). Localization of cytochromes to the outer membrane of anaerobically grown Shewanella putrefaciens MR-1. *Journal of Bacteriology, 174*(11), 3429-3438.

Myers, C. R., & Nealson, K. H. (1988). Microbial reduction of manganese oxides: Interactions with iron and sulfur. *Geochimica et Cosmochimica Acta, 52*(11), 2727-2732.

Myers, J. M., & Myers, C. R. (2001). Role for outer membrane cytochromes OmcA and OmcB of Shewanella putrefaciens MR-1 in reduction of manganese dioxide. *Applied and environmental microbiology, 67*(1), 260-269.

Myland, J. C., & Oldham, K. B. (1990). Diffusion-limited currents at hemispheroidal microelectrodes. *Journal of Electroanalytical Chemistry and Interfacial Electrochemistry, 288*(1-2), 1-14.

Newman, D. K., & Kolter, R. (2000). A role for excreted quinones in extracellular electron transfer. *Nature, 405*(6782), 94-97.

Nyholm, L., & Wikmark, G. (1993). Anodic stripping voltammetry of copper at ex situ-formed mercury-coated carbon fiber microelectrodes in the presence of low concentrations of supporting electrolyte. *Analytica Chimica Acta, 273*(1-2), 41-51.

Paik, C. H., & Alkire, R. C. (2001). Role of sulfide inclusions on localized corrosion of Ni200 in NaCl solutions. *Journal of the Electrochemical Society, 148*(7), B276-B281.

Paik, C. H., White, H. S., & Alkire, R. C. (2000). Scanning electrochemical microscopy detection of dissolved sulfur species from inclusions in stainless steel. *Journal of the Electrochemical Society, 147*(11), 4120-4124.

Rozan, T. F., Theberge, S. M., & Luther, G. (2000). Quantifying elemental sulfur (S0), bisulfide (HS-) and polysulfides (Sx2-) using a voltammetric method. *Analytica Chimica Acta, 415*(1-2), 175-184.

Rudolph, D., Bates, D., DiChristina, T., Kranz, C., Mizaikoff, B. (2005). Detection of Metal-Reducing Enzyme Complexes by Scanning Electrochemical Microscopy (SECM). *Nature Methods*, in preparation.

Rudolph, D., Neuhuber, S., Kranz, C., Taillefert, M., & Mizaikoff, B. (2004). Scanning electrochemical microscopy imaging of rhodochrosite dissolution using gold amalgam microelectrodes. *Analyst (Cambridge, United Kingdom), 129*(5), 443-448.

Saito, Y. (1968). Theoretical study on the diffusion current at the stationary electrodes of circular and narrow band types. *Review of Polarography, 15*(6), 177-187.

Schaegger, H., Cramer, W. A., & von Jagow, G. (1994). Analysis of molecular masses and oligomeric states of protein complexes by blue native electrophoresis and isolation of membrane protein complexes by two-dimensional native electrophoresis. *Analytical Biochemistry, 217*(2), 220-230.

Schaegger, H., & Von Jagow, G. (1991). Blue native electrophoresis for isolation of membrane protein complexes in enzymically active form. *Analytical Biochemistry, 199*(2), 223-231.

Schreyer, A., Suter, T., Eng, L., & Bohni, H. (1998). Local probing of electrochemical interfaces in corrosion research. *Electrochemical Nanotechnology*, 199-213.

Seelig, P. F., & Blount, H. N. (1979). Application of recursive estimation to the real time analysis of trace metal analytes by linear sweep, pulse, and differential pulse anodic stripping voltammetry. *Analytical Chemistry, 51*(8), 1129-1134.

Selzer, Y., & Mandler, D. (2000). Scanning Electrochemical Microscopy. Theory of the Feedback Mode for Hemispherical Ultramicroelectrodes: Steady-State and Transient Behavior. *Analytical Chemistry, 72*(11), 2383-2390.

Shao, Y., & Mirkin, M. V. (1998). Probing Ion Transfer at the Liquid/Liquid Interface by Scanning Electrochemical Microscopy (SECM). *J. Phys. Chem. B, 102*(49), 9915-9921.

Still, J. W., & Wipf, D. O. (1997). Breakdown of the iron passive layer by use of the scanning electrochemical microscope. *Journal of the Electrochemical Society, 144*(8), 2657-2665.

Stojek, Z., & Kublik, Z. (1975). Silver based mercury film electrode. I. General characteristics and stability of the electrode. *Journal of Electroanalytical Chemistry and Interfacial Electrochemistry, 60*(3), 349-358.

Taillefert, M., Luther, G. W., III, & Nuzzio, D. B. (2000). The application of electrochemical tools for in situ measurements in aquatic systems. *Electroanalysis, 12*(6), 401-412.

Tercier, M.-L., Buffle, J., & Graziottin, F. (1998). A novel voltammetric in situ profiling system for continuous real-time monitoring of trace elements in natural waters. *Electroanalysis, 10*(6), 355-363.

Tercier, M. L., Parthasarathy, N., & Buffle, J. (1995). Reproducible, reliable and rugged Hg-plated Ir-based microelectrode for in situ measurements in natural waters. *Electroanalysis, 7*(1), 55-63.

Thamdrup, B., Rossello-Mora, R., & Amann, R. (2000). Microbial manganese and sulfate reduction in Black Sea shelf sediments. *Applied and Environmental Microbiology, 66*(7), 2888-2897.

Theberge, S. M., & Luther, G. W., III. (1997). Determination of the electrochemical properties of a soluble aqueous FeS species present in sulfidic solutions. *Aquatic Geochemistry, 3*(3), 191-211.

Vydra, F., & et al. (1976). *Electrochemical Stripping Analysis*.

Wechter, C., & Osteryoung, J. (1989). Square wave and linear scan anodic stripping voltammetry at iridium-based mercury film electrodes. *Analytical Chemistry, 61*(18), 2092-2097.

Wipf, D. O. (1994). Initiation and study of localized corrosion by scanning electrochemical microscopy. *Colloids and Surfaces, A: Physicochemical and Engineering Aspects, 93*, 251-261.